Article

Cell Reports

PRMT6 Regulates RAS/RAF Binding and MEK/ERK-Mediated Cancer Stemness Activities in Hepatocellular Carcinoma through CRAF Methylation

Graphical Abstract

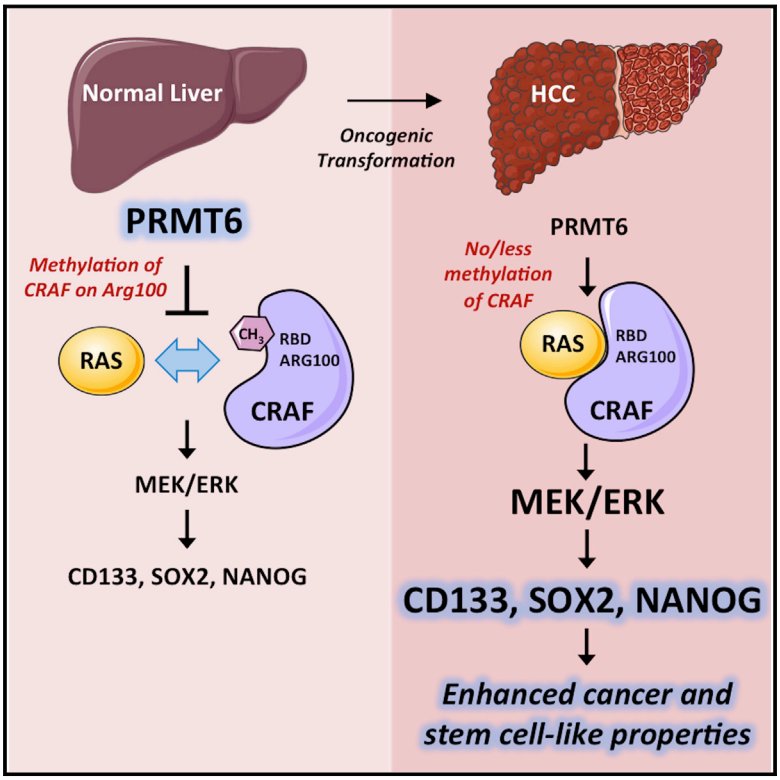

Highlights

- PRMT6 is downregulated in HCC and correlates negatively with aggressive HCC
- PRMT6 silencing drives cancer stemness *in vitro* and patient-derived organoids
- PRMT6 binds to CRAF, methylates it, and interferes with its RAS/RAF binding
- Methylation of CRAF regulates MEK/ERK-mediated cancer stemness in HCC

Authors

Lok Hei Chan, Lei Zhou, Kai Yu Ng, ..., Xin-Yuan Guan, Michael S.Y. Huen, Stephanie Ma

Correspondence

stefma@hku.hk

In Brief

RAS/RAF/MEK/ERK pathway signaling is known to be frequently activated in cancers, in which it regulates cell growth, malignant transformation, drug resistance, and stemness. Using hepatocellular carcinoma as a model system, Chan et al. describe a mechanism by which this oncogenic signaling pathway is regulated by PRMT6 at the post-translational level via arginine methylation.

Chan et al., 2018, Cell Reports *25*, 690–701
October 16, 2018
https://doi.org/10.1016/j.celrep.2018.09.053

CellPress

OPEN ACCESS
CellPress

Cell Reports
Article

PRMT6 Regulates RAS/RAF Binding and MEK/ERK-Mediated Cancer Stemness Activities in Hepatocellular Carcinoma through CRAF Methylation

Lok Hei Chan,[1,11] Lei Zhou,[1,11] Kai Yu Ng,[1,11] Tin Lok Wong,[1,11] Terence K. Lee,[7] Rakesh Sharma,[2] Jane H. Loong,[1] Yick Pang Ching,[1,3] Yun-Fei Yuan,[8] Dan Xie,[8] Chung Mau Lo,[3,5] Kwan Man,[3,5] Benedetta Artegiani,[9] Hans Clevers,[9] Helen H. Yan,[6] Suet Yi Leung,[6] Stéphane Richard,[10] Xin-Yuan Guan,[3,4] Michael S.Y. Huen,[1] and Stephanie Ma[1,3,12,*]

[1]School of Biomedical Sciences, University of Hong Kong, Pokfulam, Hong Kong, China
[2]Proteomics & Metabolomics Core Facility, Li Ka Shing Faculty of Medicine, University of Hong Kong, Pokfulam, Hong Kong, China
[3]State Key Laboratory for Liver Research, University of Hong Kong, Pokfulam, Hong Kong, China
[4]Department of Clinical Oncology, University of Hong Kong, Queen Mary Hospital, Pokfulam, Hong Kong, China
[5]Department of Surgery, University of Hong Kong, Queen Mary Hospital, Pokfulam, Hong Kong, China
[6]Department of Pathology, University of Hong Kong, Queen Mary Hospital, Pokfulam, Hong Kong, China
[7]Department of Applied Biology & Chemical Technology, Hong Kong Polytechnic University, Hong Kong, China
[8]State Key Laboratory of Oncology in Southern China, Sun Yat-Sen University Cancer Centre, Guangzhou, China
[9]Hubrecht Institute for Developmental Biology and Stem Cell Research, University Medical Centre Utrecht, Utrecht, the Netherlands
[10]Lady Davis Institute, Jewish General Hospital, and Departments of Oncology and Medicine, McGill University, Montreal, QC, Canada
[11]These authors contributed equally
[12]Lead Contact
*Correspondence: stefma@hku.hk
https://doi.org/10.1016/j.celrep.2018.09.053

SUMMARY

Arginine methylation is a post-translational modification that plays pivotal roles in signal transduction and gene transcription during cell fate determination. We found protein methyltransferase 6 (PRMT6) to be frequently downregulated in hepatocellular carcinoma (HCC) and its expression to negatively correlate with aggressive cancer features in HCC patients. Silencing of PRMT6 promoted the tumor-initiating, metastasis, and therapy resistance potential of HCC cell lines and patient-derived organoids. Consistently, loss of PRMT6 expression aggravated liver tumorigenesis in a chemical-induced HCC PRMT6 knockout (*PRMT6*$^{-/-}$) mouse model. Integrated transcriptome and protein-protein interaction studies revealed an enrichment of genes implicated in RAS signaling and showed that PRMT6 interacted with CRAF on arginine 100, which decreased its RAS binding potential and altered its downstream MEK/ERK signaling. Our work describes a critical repressive function for PRMT6 in maintenance of HCC cells by regulating RAS binding and MEK/ERK signaling via methylation of CRAF on arginine 100.

INTRODUCTION

Post-translational modifications lie at the heart of the fields of epigenetics and signal transduction. Arginine methylation is a common post-translational modification functioning as an epigenetic machinery of transcription and playing key roles in mRNA translation, cell signaling, and cell fate decision. In mammals, arginine methylation is carried out by protein arginine methyltransferases (PRMTs) (Bedford and Clarke, 2009; Blanc and Richard, 2017). Recent studies have defined physiological roles of PRMTs, linking them to diseases such as cancer and metabolic disorders. PRMT6 belongs to the type I PRMT enzyme family, responsible for catalyzing the asymmetric dimethylation of arginine (ADMA) residues on proteins (Blanc and Richard, 2017). It was initially identified to modify GAR motifs and subsequently found to target histones, although non-histone targets have also been described (Frankel et al., 2002; Guccione et al., 2007; Iberg et al., 2008; Hyllus et al., 2007; Di Lorenzo et al., 2014). The role of PRMT6 in normal and cancer cell remains controversial. It has been reported to function as both a transcriptional repressor and activator and be overexpressed and repressed in different tumor types. Reduced PRMT6 expression has been reported in melanoma (Limm et al., 2013), while overexpression of PRMT6 is detected in cancers of the bladder, lung, cervix, breast, and prostate (Almeida-Rios et al., 2016; Yoshimatsu et al., 2011). Importantly, studies on PRMT6 to date have only been focused on its function in the nucleus. The biological significance and the key target proteins of PRMT6 in human cancer remains elusive.

Hepatocellular carcinoma (HCC) remains one of the most prevalent and deadliest cancer types in the world. Resection and transplantation is remedial for early-stage HCC. Yet because most patients are diagnosed at an advanced stage, most HCCs are inoperable. Chemotherapy and molecular targeted therapies are available for advanced HCC patients, but their effects have shown only modest results. HCC tumors are heterogeneous and contain cells that sit at the apex of cellular hierarchies with stem-like properties. These HCC stem-like cells can self-renew, are resistant to conventional therapy, and can

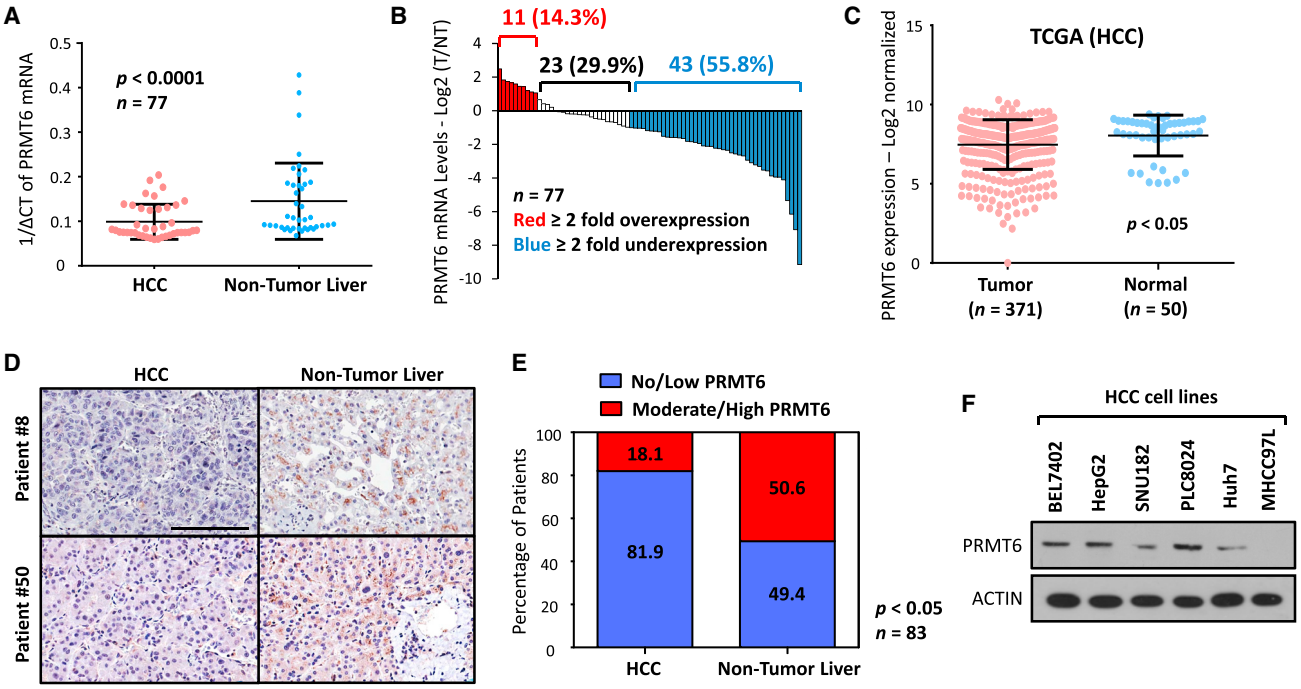

Figure 1. PRMT6 Is Weakly Expressed and Negatively Correlated with Aggressive Cancer Features in HCC Patients

(A and B) Scattered dot (A) and waterfall (B) plot analyses of PRMT6 mRNA levels in HCC and matched non-tumor liver specimens from 77 patient samples. Red and blue bars represent samples that show a relative PRMT6 fold change of ≥2 overexpression and underexpression, respectively (HCC/NT).

(C) Scattered dot plot analysis of PRMT6 mRNA levels in normal (n = 50) and HCC (n = 371) tissues using information gathered from the TCGA HCC dataset.

(D) PRMT6 immunostaining of tissue microarray comprising 83 paired non-tumor liver and HCC tissue samples. Shown are representative images of the immunostaining. Scale bar, 100 μm.

(E) Graph indicates the percentage of cases displaying no and/or low or moderate and/or high staining intensity of PRMT6.

(F) Proteomic expression of PRMT6 in HCC cell lines by western blot.

Data are representative of two or more independent experiments. Bars and error represent mean ± SD of replicate measurements.

contribute to tumor recurrence (Yamashita and Wang, 2013). Treatment of HCC with chemotherapy has been found to select for the outgrowth of therapy-resistant stem-like cancer cells that contribute to tumor recurrence and poor therapeutic outcome (Visvader and Lindeman, 2012). This underscores the need for a better understanding of the molecular mechanisms driving stemness in HCC cells in hope to discover features that may render HCC cells with stem-like properties more susceptible to selective therapeutic intervention.

RAF kinases are well-known oncoproteins that play a critical role in promoting cancer through activation of the MEK/ERK signaling cascade (Lavoie and Therrien, 2015). In recent years, MEK/ERK activation has been extensively reported to be essential for mediating the self-renewal capacity and drug-resistant properties of HCC cells, leading to poor patient survival. Activation of the RAS/RAF/MEK/ERK cascade is observed in 50%–100% of HCC tumors (Ito et al., 1998), yet activating mutations of RAS/RAF are infrequent, with downregulation of inhibitory regulators of the pathway being the more common alternative mechanism leading to activation of MEK/ERK. Although the presence of repressive elements in RAF has been long recognized, they cannot account for all MEK/ERK activations in HCC, while post-translational modifications other than phosphorylation that control RAF kinase activity remains elusive. A broader understanding of how negative regulatory effectors on this signaling pathway are deregulated in HCC is important for future development of anti-cancer strategies. Our present study uncovered the clinical significance and functional role of PRMT6 in mediating HCC stemness and dissected the molecular mechanism by which PRMT6 contributes to these effects via interaction and methylation of CRAF on arginine 100.

RESULTS

PRMT6 Is Weakly Expressed and Negatively Correlated with Aggressive Cancer Features in HCC Patients

We investigated PRMT6 mRNA expression in 77 primary HCC and matched non-tumor liver tissues using qPCR. PRMT6 downregulation of ≥2-fold was displayed in 55.8% (43 of 77) of the HCC specimens compared with non-tumor specimens (Figures 1A and 1B). Analysis of a publicly available dataset (The Cancer Genome Atlas [TCGA], Liver Cancer) also showed PRMT6 downregulation in HCC compared with normal liver samples (Figure 1C). These observations were further validated by immunohistochemistry (IHC) in a separate cohort consisting of 83 primary HCC and adjacent non-tumor tissue (Figures 1D and 1E), in which PRMT6 downregulation in HCC was

significantly associated with older age (p = 0.025), presence of vascular invasion (p = 0.035), intraoperative rupture (p = 0.049), and a trend toward absent or incomplete tumor encapsulation (p = 0.053) (Table S1). Different PRMT6 antibodies were used for IHC, including one validated by the Human Protein Atlas, to provide further confidence to our work (Figure S1). Expression of PRMT6 was also tested in HCC cell lines for selecting cell lines for subsequent functional studies (Figure 1F).

PRMT6 Negatively Regulates Cancer and Stem Cell-like Properties in HCC

To determine the pathological role of PRMT6 in HCC, we ablated PRMT6 expression in BEL7402 with two distinct short hairpin RNAs (shRNAs) (933 and 956) and stably overexpressed PRMT6 in Huh7 and/or MHCC97L cells (Figures S2A–S2C). Knockdown of PRMT6 resulted in attenuated PRMT6 expression but not other members of the PRMT family, providing evidence that the effects observed are due solely to PRMT6 (Figure S2D). PRMT6 depletion led to potentiated ability of the cells to migrate, invade, and resist cisplatin, 5-fluorouracil, and sorafenib. Conversely, stable PRMT6 overexpression in Huh7 cells resulted in opposing effects (Figures 2A and 2B). We extended our studies *in vivo*, in which HCC cells with PRMT6 manipulated were injected subcutaneously or orthotopically into nude mice to determine the role of PRMT6 in HCC formation. Overexpression of PRMT6 resulted in a profound decrease in the ability of cells to initiate tumor growth, while knockdown of PRMT6 led to a marked induction (Figures 2C and 2D). We also examined the role of PRMT6 in HCC metastasis *in vivo* by orthotopic implantation of HCC cells into the livers of immunodeficient mice. Because BEL7402 and Huh7 cells are known to be unable to form metastases following intrahepatic injection, luciferase-labeled MHCC97L cells overexpressing empty vector (EV) or PRMT6 were used instead. Extrahepatic lung metastasis was monitored by *ex vivo* bioluminescence imaging, and metastasis was detected in four of six mice in the EV group, in contrast to only two of six mice in the PRMT6 overexpression group (Figure 2E), with a faster metastasis onset. Altered ability of the cells to metastasize was also evident by a decreased number of tumor nodules present in the lung of mice injected with PRMT6 overexpressing cells (Figure 2E).

PRMT6 negatively regulated not only aggressive cancer features but also stem-like properties of HCC. HCC cells with PRMT6 overexpressed displayed attenuated abilities to induce oncosphere formation in serial passages (Figure 3A), as well as reduced expression of CD133 HCC stem-like subpopulation (Figure 3B) and pluripotency markers SOX2 and NANOG (Figure 3C). Knockdown of PRMT6 resulted in an opposing trend (Figures 3A and 3C). Note expression of other liver cancer stem cell (CSC) markers such as CD24 and CD90 were not found to be altered following PRMT6 expression modulation (Figure S2F). To assess the degree to which PRMT6 supports growth and maintenance of $CD133^+$ HCC stem-like cells, Huh7 cells overexpressing EV ($PRMT6^{low}$) or PRMT6 ($PRMT6^{high}$) were sorted into $CD133^+$ and $CD133^-$ subsets and injected into NOD/SCID mice at limiting dilutions. Mice injected with $CD133^+PRMT6^{low}$ cells showed increased tumor incidence, expedited tumor latency, and a higher frequency of tumor-initiating cells compared with other subgroups (Figure 3D). Self-renewal ability of cells was then examined by serial transplantation of primary xenografts into secondary mouse recipients. Single cells isolated from the four groups were resorted into $CD133^+$ and $CD133^-$ subsets and injected at limiting dilutions. $CD133^+PRMT6^{low}$ cells displayed further expedited tumor latency in their ability to reconstitute tumor formation in secondary transplantations. Statistically, HCC cells with low PRMT6 showed a significantly worse tumor-free survival compared with HCC cells with high PRMT6 expression ($CD133^+$ $PRMT6^{low}$ versus $CD133^+PRMT6^{high}$) in serial transplantations (Figure 3D). Note that because BEL7402 cells do not express any endogenous CD133, we were unable to analyze change in CD133 expression and sort CD133 subpopulation for *in vivo* assays as we did for Huh7. Note that similar results were also achieved in BEL7402 cells with PRMT6 knocked out by CRISPR/Cas9, suggesting that the observed effects are due solely to PRMT6 and not other members of the PRMT family (Figure S2E).

The Catalytically Active Domain of PRMT6 Is Functionally Important in Contributing Augmented Cancer Stemness Properties in HCC

Lentiviral-based knockdown and overexpression of PRMT6 led to a concomitant respective decrease and increase of ADMA (Figure 4A), suggesting that the global arginine methyltransferase activity of these cells was altered. To examine whether PRMT6 confers altered cancer stemness properties in HCC through this enzymatic activity, we performed similar functional studies with wild-type PRMT6 or catalytic methyltransferase inactive mutant $PRMT6^{VLD:KLA}$ (Neault et al., 2012) overexpressed in BEL7402 HCC cells (Figure 4B). Ectopic overexpression of wild-type and catalytic inactive PRMT6 mutant displayed predominant cytoplasmic PRMT6 localization (Figure S3). Functionally, wild-type PRMT6 overexpression conferred the ability of HCC cells to diminish migration, invasion, and oncosphere formation (Figures 4C–4E). Furthermore, it led to attenuated ability of the cells to resist cisplatin, 5-fluorouracil, and sorafenib as well as a reduced expression of SOX2 (Figures 4C–4G). Overexpression of wild-type PRMT6 also resulted in a decrease in the ability of the cells to initiate tumors *in vivo* (Figure 4H). In contrast, a catalytic methyltransferase inactive mutant of PRMT6 was unable to confer such functional phenotype.

PRMT6 Interacts Directly with CRAF

Contrary to what is reported in the literature for other tumor types, we found modulation of PRMT6 to not play a very significant or consistent role in H3R2 methylation, at least in the context of HCC, as evidenced by both H3R2me2a expression and chromatin immunoprecipitation (ChIP)-qPCR experiments on promoter regions of p21, p27, and p57, previously reported to be regulated by H3R2me2a, coupled with expression analysis of p21, p27, and p57 extracted from our microarray data (Figure S4). More importantly, PRMT6 is predominantly expressed in the cytoplasm of HCC cells (Figure S5). To ensure that our observation was HCC specific, we performed the same immunofluorescence experiment using two PRMT6 antibodies and with MCF7 breast cancer cells, which have previously been reported to express only nuclear PRMT6 (Hyllus et al., 2007), as

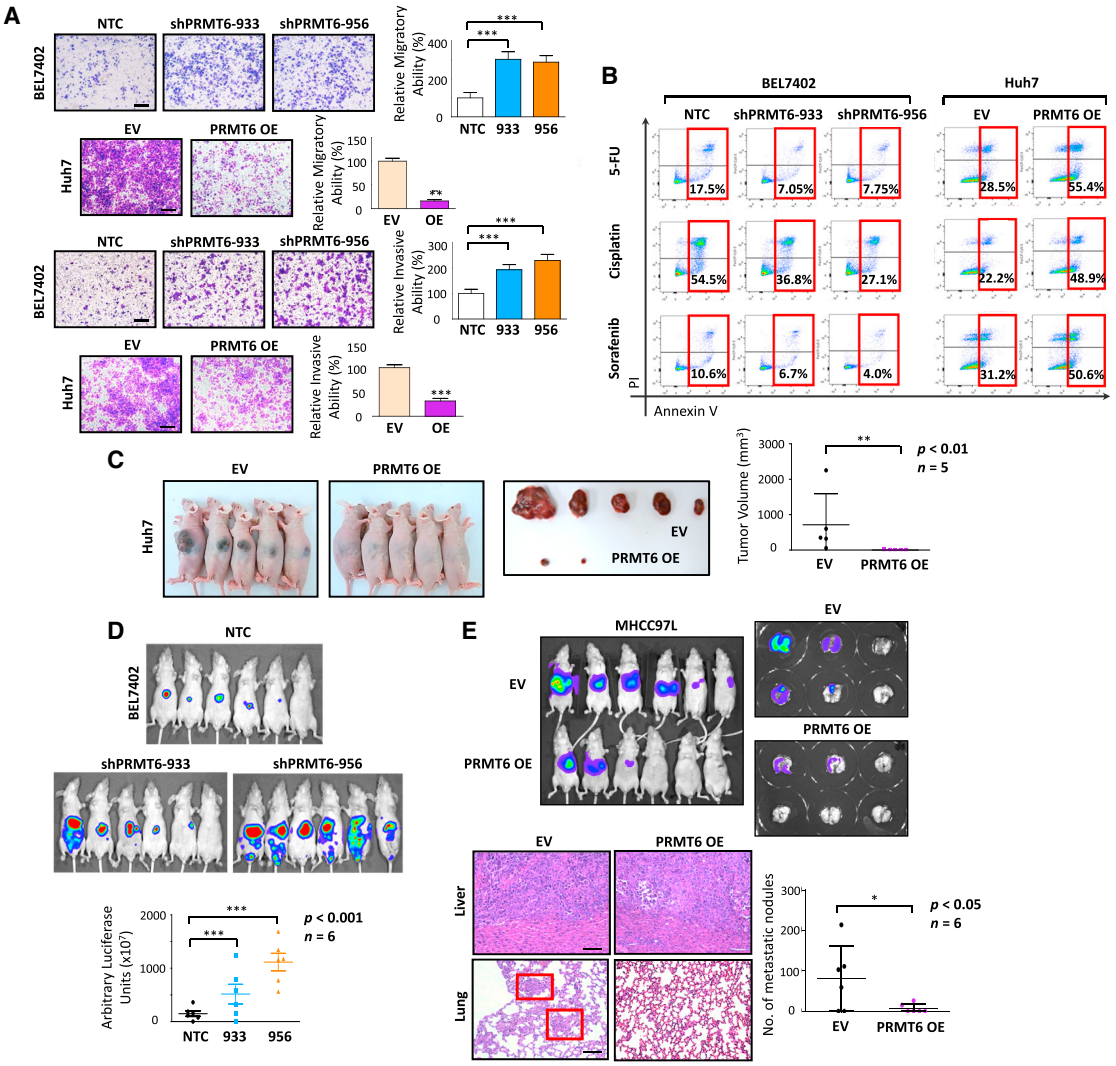

Figure 2. PRMT6 Negatively Regulates Cancer Properties in HCC

(A) Representative images and quantification of number of cells that migrated and invaded in BEL7402 and Huh7 cells with or without PRMT6 expression modulated. **p < 0.01 and ***p < 0.001. Scale bar, 100 μm.

(B) Percentage of annexin V-PI-positive cells in BEL7402 and Huh7 cells with or without PRMT6 expression modulated in the presence of 5-flurouracil, cisplatin, or sorafenib.

(C) Xenograft tumors and tumor volume measurements of Huh7 cells with or without PRMT6 overexpressed.

(D) Bioluminescence imaging and luciferase signal quantification of nude mice injected intrahepatically with luciferase-labeled BEL7402 cells with or without PRMT6 suppressed.

(E) *In vivo* bioluminescence imaging of nude mice injected intrahepatically with luciferase-labeled MHCC97L cells with or without PRMT6 overexpressed. *Ex vivo* imaging of the lungs harvested. Representative H&E images of liver and lung tissues harvested. Scale bar, 100 μm. Bar chart summary of number of metastatic foci observed in lung.

EV, empty vector control; NTC, non-target control; OE, overexpression. Data are representative of two or more independent experiments. Bars and error represent mean ± SD of replicate measurements.

a positive control, with findings in support of our hypothesis (Figure S5). To elucidate the underlying mechanism of PRMT6 in the regulation of HCC stem-like cells, we used an integrative approach whereby we sought to identify both downstream altered genes and potential binding partners of PRMT6, hoping to identify members of the pathway that are regulated via arginine methylation. mRNA profiling of HCC cells with or without PRMT6 stably suppressed identified significantly deregulated genes that closely associated with RAS signaling and aggressive cancer phenotypes, including epithelial-mesenchymal transition (Figures 5A and S6; Table S2). Tandem affinity purification coupled with mass spectrometry (TAP-MS) analysis of PRMT6 immunoprecipitates identified a list of PRMT6-interacting proteins. Through integrating mRNA profiling and TAP-MS analysis,

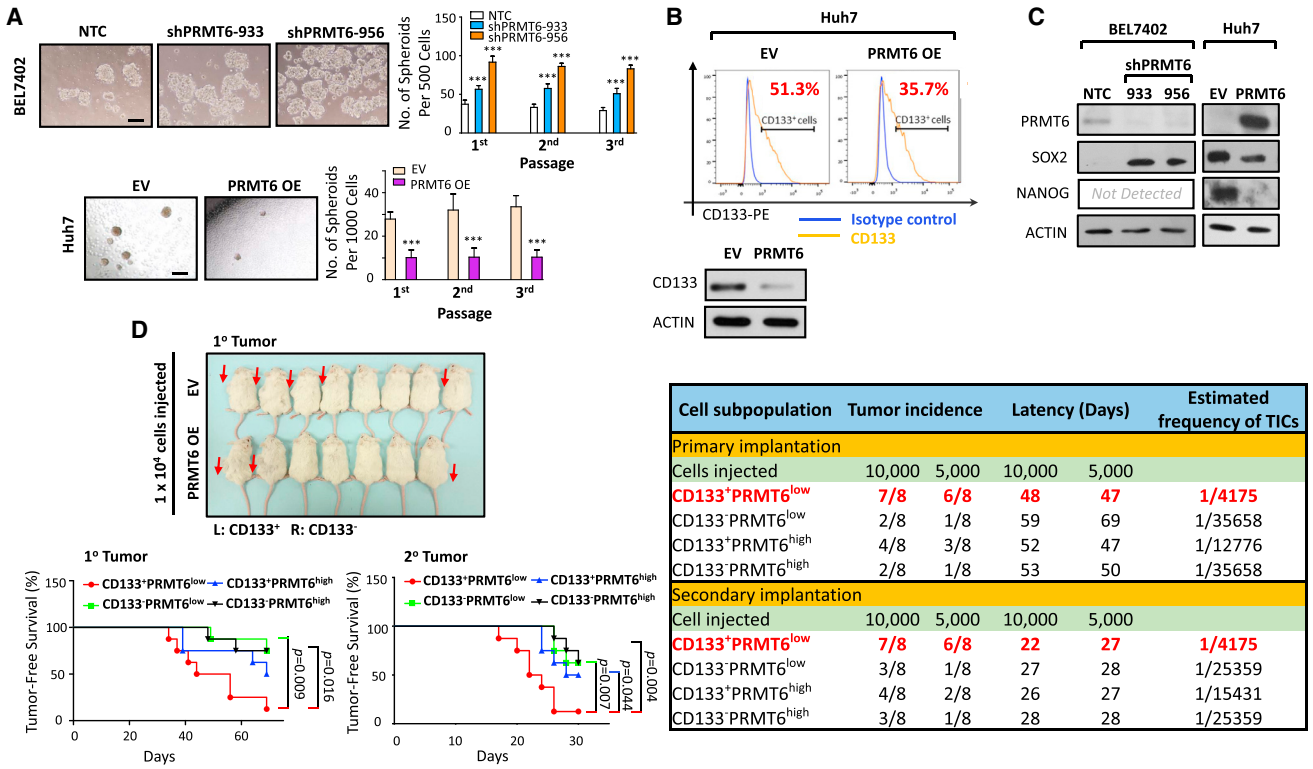

Cell subpopulation	Tumor incidence		Latency (Days)		Estimated frequency of TICs
Primary implantation					
Cells injected	10,000	5,000	10,000	5,000	
CD133⁺PRMT6^{low}	**7/8**	**6/8**	**48**	**47**	**1/4175**
CD133⁻PRMT6^{low}	2/8	1/8	59	69	1/35658
CD133⁺PRMT6^{high}	4/8	3/8	52	47	1/12776
CD133⁻PRMT6^{high}	2/8	1/8	53	50	1/35658
Secondary implantation					
Cell injected	10,000	5,000	10,000	5,000	
CD133⁺PRMT6^{low}	**7/8**	**6/8**	**22**	**27**	**1/4175**
CD133⁻PRMT6^{low}	3/8	1/8	27	28	1/25359
CD133⁺PRMT6^{high}	4/8	2/8	26	27	1/15431
CD133⁻PRMT6^{high}	3/8	1/8	28	28	1/25359

Figure 3. PRMT6 Negatively Regulates Cancer Stemness Properties in HCC

(A) Oncosphere formation and serial passages of BEL7402 and Huh7 cells with or without PRMT6 expression modulated. ***$p < 0.001$. Scale bar, 100 μm.

(B) Flow cytometry and western blot analyses for CD133 expression in Huh7 cells with or without PRMT6 overexpressed.

(C) Western blot analysis for PRMT6, SOX2, and NANOG expression in BEL7402 and Huh7 cells with or without PRMT6 expression modulated.

(D) Images of xenograft tumors (red arrows) formed in NOD/SCID mice injected subcutaneously with CD133⁺PRMT6^{low}, CD133⁺PRMT6^{high}, CD133⁻PRMT6^{low}, and CD133⁻PRMT6^{high} cells isolated from Huh7 cells in primary passage (picture representative of 10,000 cells injected). Kaplan-Meier curves showing percentage of tumor-free survival of the annotated groups of primary and secondary recipient mice. n = 8. Engraftment rates, average tumor latency, and tumor-initiating frequency of CD133⁺ and CD133⁻ subsets with or without PRMT6 overexpressed in Huh7 cells.

EV, empty vector control; NTC, non-target control; OE, overexpression; TIC, tumor-initiating cells. Data are representative of two or more independent experiments. Bars and error represent mean ± SD of replicate measurements.

we shortlisted 11 RAS signaling-related proteins that potentially bind to PRMT6, including RAF1/CRAF (Table S3). Downstream signaling of CRAF, namely, MEK/ERK, has previously been shown by us and others to promote stem cell-like properties in HCC, and thus we hypothesized that PRMT6 regulates HCC stem-like cell via binding to CRAF and altering downstream MEK/ERK signaling. To test our hypothesis, we first confirmed the interaction between PRMT6 and CRAF by reciprocal immunoprecipitations in 293T and HCC cells, using both tagged and endogenous proteins (Figure 5B). Following confirmation of their binding, we then examined for the presence of PRMT6-mediated enzymatic methylation of CRAF by *in vivo* methylation assay. Levels of ADMA were drastically increased when PRMT6 plasmid was co-transfected relative to EV control (Figure 5C, left). To further provide direct evidence in support of CRAF as a specific PRMT6 substrate, *in vitro* methylation assay was then carried out, alongside a glycine-arginine-rich (GAR) sequence as a positive control. In the presence of PRMT6, methylation of CRAF was dramatically potentiated (Figure 5C, middle and right).

PRMT6 Methylates CRAF on Arginine 100 Residue

An *in silico* analysis of the CRAF protein sequence by PMeS prediction revealed seven arginine residues that could be potentially methylated (Table S4). To identify which arginine residues are methylated by PRMT6, we created full-length and multiple truncated mutants of CRAF (Figure 5D). When CRAF full-length (FL) and truncated mutants (D1–D3) were co-transfected with PRMT6 into 293T cells for *in vivo* methylation assay, ADMA at the predicted size (red arrows) could be detected in FL CRAF as well as D1 and D3 truncated CRAF, where arginine residues 89 and 100 are present. In contrast, the predicted ADMA band could not be detected in D2 truncated CRAF, where arginine 89 and 100 residues are deleted (Figure 5E, white arrow). These observations indicated that arginine 89 and 100 in CRAF were the potential targets of PRMT6. *In vivo* and *in vitro* methylation assays using site-directed R89K and R100K CRAF mutants showed that only R100 was specifically methylated by PRMT6 (Figure 5F). This was further confirmed by *in vitro* methylation assays using peptide overlying nine amino acids around R100 residue (CAVFRLLHE) or with R→K substitution (CAVFKLLHE),

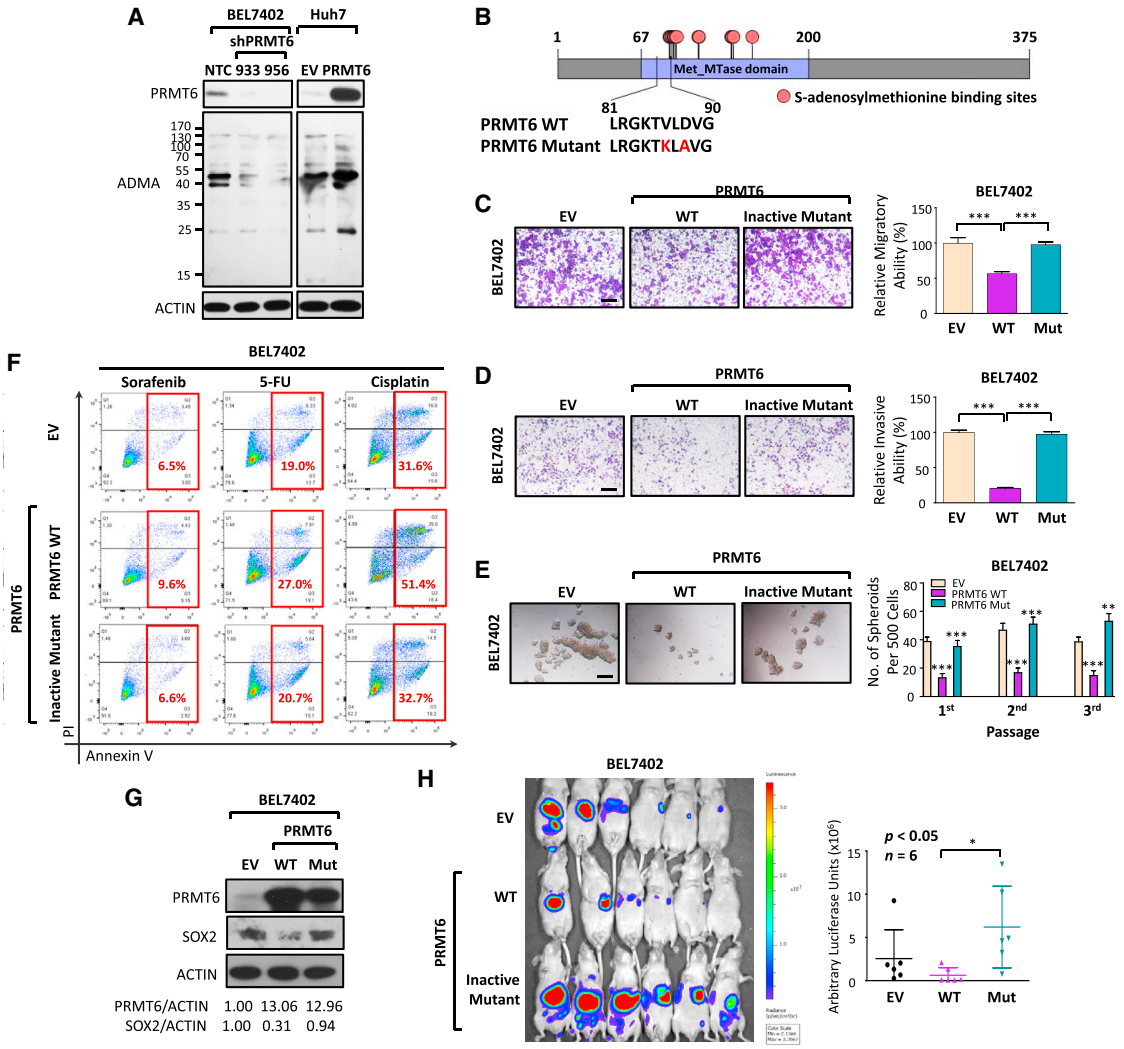

Figure 4. The Catalytically Active Domain of PRMT6 Is Functionally Important in Contributing Augmented Aggressive Cancer Stemness Properties in HCC

(A) Western blot analysis for ADMA expression in BEL7402 and Huh7 cells with or without PRMT6 expression modulated.

(B) Schematic illustration of PRMT6 wild-type (WT) and PRMT6 catalytic inactive (mutant) constructs used in this study.

(C–E) Representative images and quantification of number of cells that (C) migrated, (D) invaded, and (E) formed oncospheres in BEL7402 cells stably over-expressing EV control, WT, and mutant PRMT6. **$p < 0.01$ and ***$p < 0.001$. Scale bar, 100 μm.

(F) Percentage of annexin V-PI-positive cells in BEL7402 cells stably overexpressing EV control, WT, and mutant in the presence of 5-flurouracil, cisplatin, or sorafenib.

(G) Western blot analysis for PRMT6, SOX2, and NANOG expression in BEL7402 cells stably overexpressing EV control, WT, and mutant PRMT6.

(H) *In vivo* bioluminescence imaging and luciferase signal quantification of nude mice injected intrahepatically with luciferase-labeled BEL7402 cells stably overexpressing EV control, WT, and mutant PRMT6.

EV, empty vector control; mut, mutant; NTC, non-target control; OE, overexpression; WT, wild-type. Data are representative of two or more independent experiments. Bars and error represent mean ± SD of replicate measurements.

showing methyl group incorporation in R100 peptide only (Figure 5G). On further analysis, we also found PRMT6 to similarly bind to other RAF family members that show high homology to CRAF, including ARAF and BRAF. Arginine residues were also predicted on ARAF and BRAF (Table S4), with R100 consistently corresponding to the 45th amino acid residue within the RAS binding domain (RBD) across all three human RAF proteins and locating within a highly conserved sequence motif consisting of six amino acids (Tables S5 and S6), suggesting the critical role of this arginine residue. The data serve as proof of concept that PRMT6 may potentially methylate ARAF and BRAF at the same arginine residue to elicit similar downstream effects, as in CRAF.

PRMT6 Methylation of CRAF at Arginine 100 Interferes with RAS/RAF Binding Domain and Inhibits MEK/ERK-Related Kinase Activity

As evidenced by western blot and kinase activity assays, knock-down of PRMT6 led to heightened MEK/ERK signaling, while

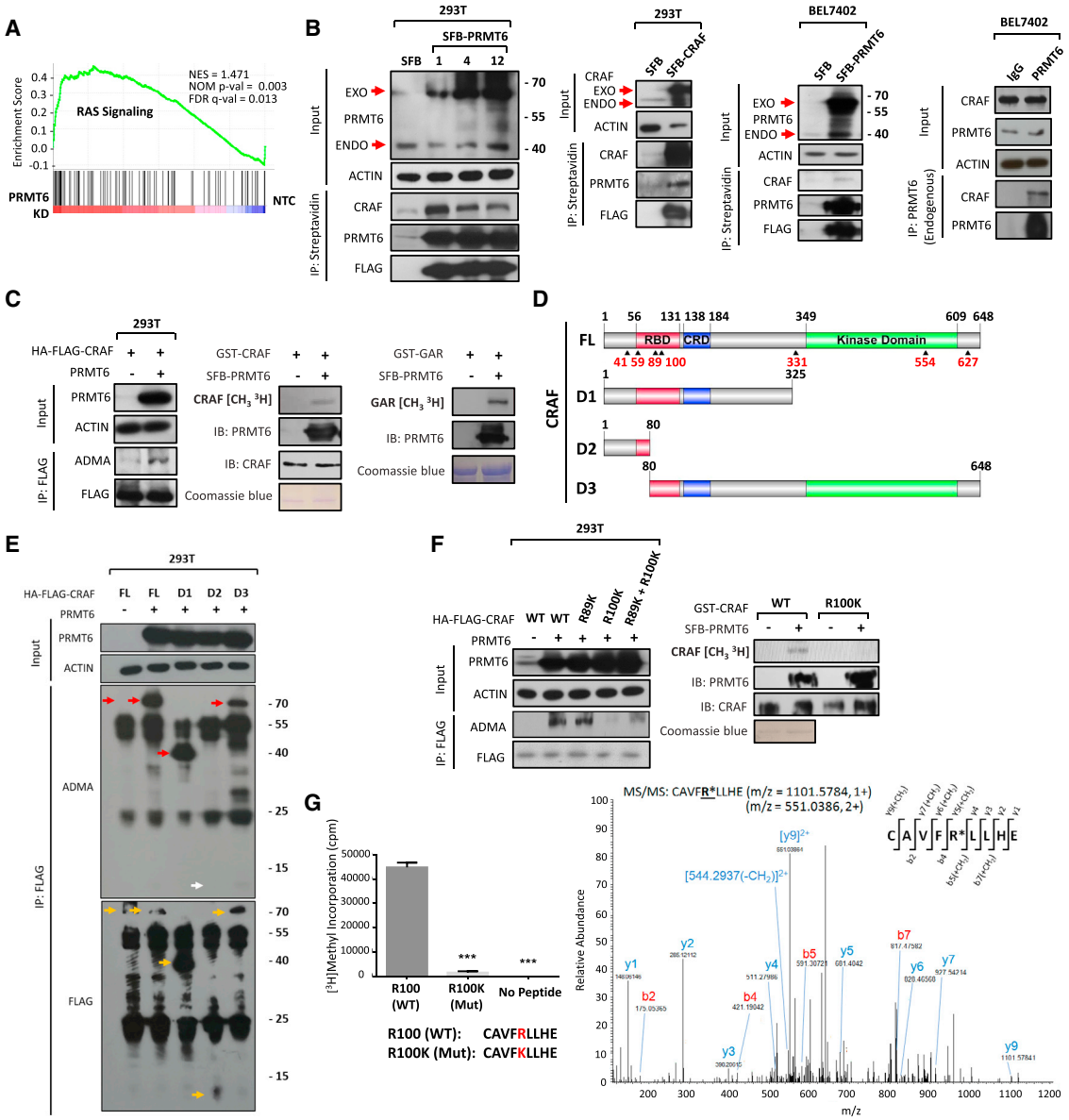

Figure 5. PRMT6 Interacts Directly with CRAF and Methylates It on Arginine 100 Residue

(A) Gene set enrichment analysis (GSEA) identified an enrichment of RAS signaling in PRMT6 silenced cells.

(B) Co-immunoprecipitation analysis for validation of CRAF as a PRMT6 interacting protein partner in 293T cells expressing SFB-tagged PRMT6, 293T cells expressing SFB-tagged CRAF, BEL7402 cells expressing SFB-tagged PRMT6, and BEL7402 expressing endogenous PRMT6.

(C) Left: western blot analysis for PRMT6-mediated incorporation of asymmetric arginine dimethylation in CRAF. Middle: western blot analysis of *in vitro* methylation assay of CRAF. Right: GAR (glycine-arginine-rich) sequence positive control in the *in vitro* methylation assay.

(D) Schematic diagram illustrating of full-length (FL) and deletion mutations of CRAF used in this study. CRD, cysteine-rich domain; RBD, Ras binding domain.

(E) Mapping of protein domain in CRAF methylated by PRMT6 through *in vivo* methylation assay. Red arrows indicate ADMA bands at the predicted size. White arrow indicates loss of ADMA band at the predicted size in D2 CRAF truncation mutant. Yellow arrows indicate successful FLAG pull-down.

(F) Left: levels of ADMA in WT and site-directed mutants of CRAF. Right: *in vitro* methylation assay of CRAF R100K mutant versus WT.

(G) Left: *in vitro* methylation assay with immunoprecipitated PRMT6 from 293T cells stably transfected with SFB-PRMT6. Assay was performed by adding no peptide, CAVFRLLHE peptide, or CAVFKLLHE mutant peptide. Right: fragmentation spectrum of the methylated peptide identified by liquid chromatography/tandem mass spectrometry (LC-MS/MS). m/z, mass/charge ratio. ***$p < 0.001$.

Endo, endogenous; Exo, exogenous; KD, knockdown; mut, mutant; NTC, non-target control; WT, wild-type. Data are representative of two or more independent experiments. Bars and error represent mean ± SD of replicate measurements.

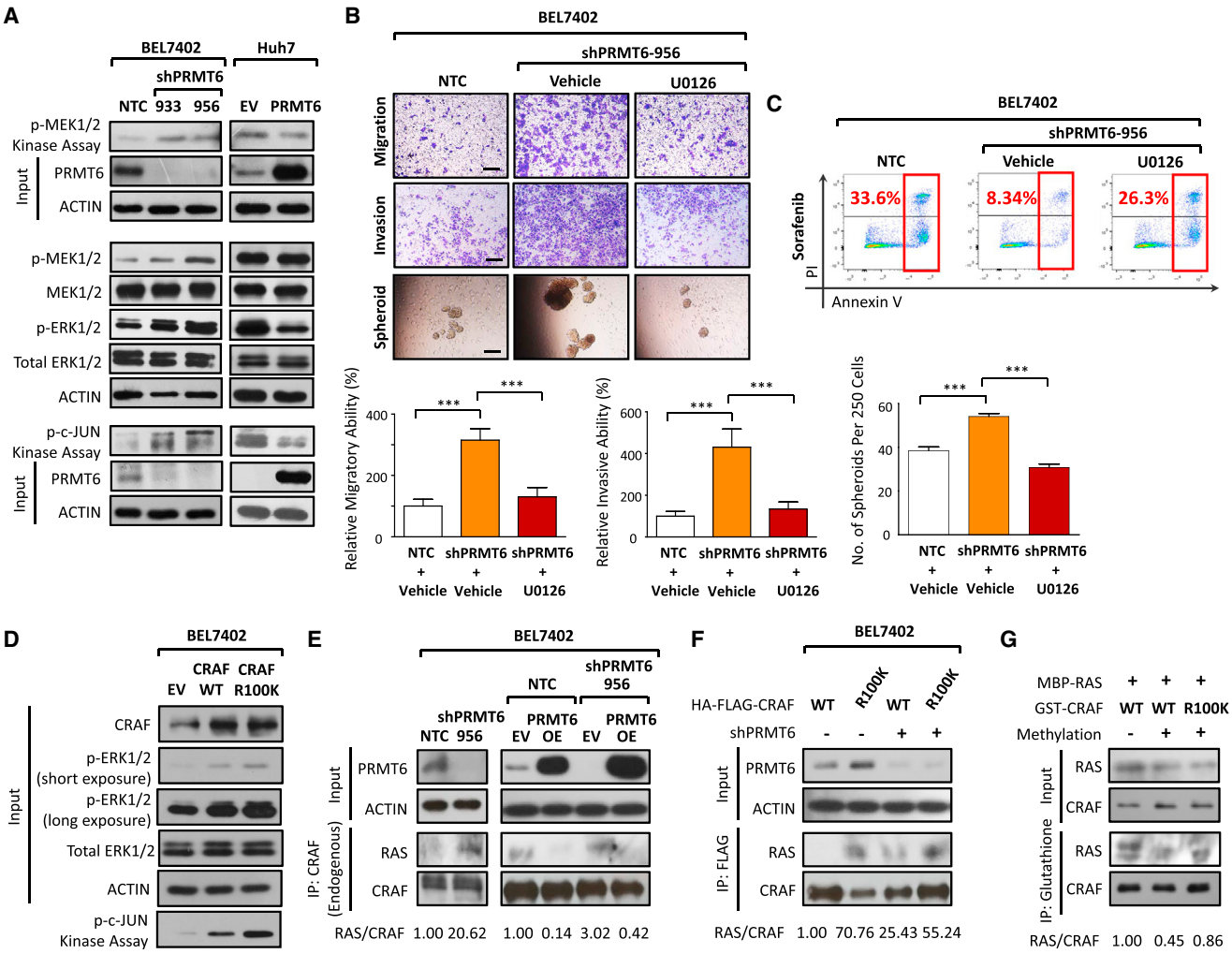

Figure 6. PRMT6 Methylation of CRAF at Arginine 100 Interferes with RAS/RAF Binding Domain and Inhibits MEK/ERK-Related Kinase Activity

(A) CRAF kinase assay, western blot analysis for expression of phosphorylated and total MEK1/2, phosphorylated and total ERK1/2 and ERK kinase assay in BEL7402 and Huh7 cells with or without PRMT6 expression modulated.

(B) Representative images and quantification of number of cells that migrated, invaded, and formed oncospheres in BEL7402 cells expressing NTC or shPRMT6 clone 956 that were treated with control or MEK inhibitor U0126. ***$p < 0.001$. Scale bar, 100 μm.

(C) Percentage of annexin V-PI-positive cells in BEL7402 cells expressing NTC or shPRMT6 clone 956 that were treated with control or MEK inhibitor U0126, following sorafenib treatment.

(D) Western blot analysis for expression of CRAF, phosphorylated and total ERK1/2, as well as ERK kinase assay in BEL7402 cells with EV control, CRAF WT, or CRAF R100K overexpressed.

(E and F) Western blot analysis for the co-immunoprecipitation of CRAF and RAS in BEL7402 cells (E) with or without PRMT6 expression modulated and (F) with CRAF WT or R100K mutant.

(G) *In vitro* methylation assay of CRAF WT and R100K mutant followed by RAS binding assay with immunoprecipitated MBP-RAS.

EV, empty vector control; NTC, non-target control; OE, overexpression; WT, wild-type. Data are representative of two or more independent experiments. Bars and error represent mean ± SD of replicate measurements.

overexpression of PRMT6 resulted in an opposing effect (Figure 6). To substantiate the importance of the MEK/ERK pathway in PRMT6-mediated HCC, we performed rescue experiments using an MEK-specific inhibitor, U0126, as well as by shERK1/2 knockdown (Figures 6B, 6C, and S7). U0126 and shERK1/2 suppressed the oncogenic properties conferred by PRMT6 knockdown, as evidenced by the diminished abilities of HCC cells to migrate, invade, form oncospheres, and resist sorafenib treatment (Figures 6B, 6C, and S7). Most important, overexpression of CRAF with R100K mutation in PRMT6 expressing BEL7402 cells led to a heightened p-ERK1/2 signal and ERK kinase activity with c-Jun as a substrate compared with wild-type CRAF (Figure 6D), demonstrating the significance of CRAF R100 residue in regulating MEK/ERK signaling. Co-immunoprecipitation of CRAF showed that shPRMT6 promoted the RAS/RAF binding, which could be inhibited by restoring PRMT6 expression

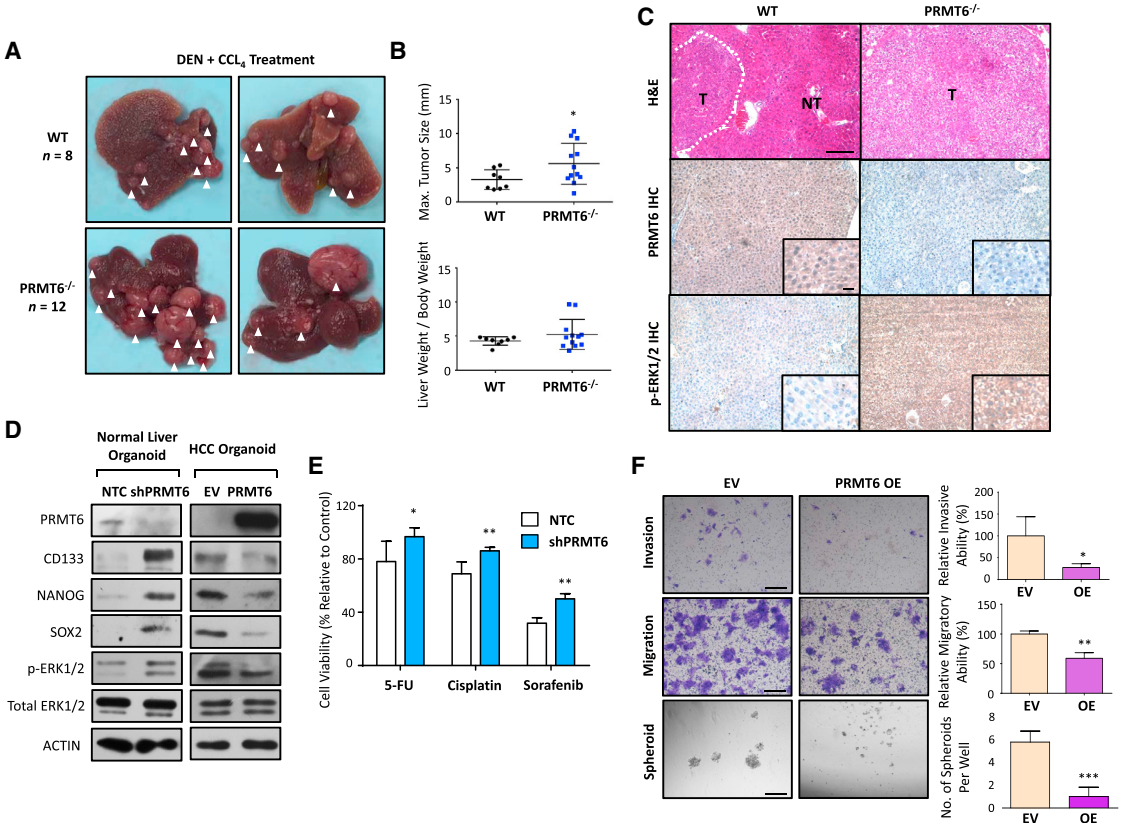

Figure 7. Loss of PRMT6 Expression Aggravates Liver Tumorigenesis in a DEN+CCL_4 HCC-Induced PRMT6 Knockout Mouse Model, and PRMT6-Dependent CRAF/ERK Signaling Regulates HCC Stemness as Demonstrated in Patient-Derived Organoids

(A) Representative pictures of livers harvested from WT and PRMT6 knockout (*PRMT6*$^{-/-}$) mice that received DEN+CCl_4 carcinogen induction.

(B) Maximum size of HCC tumors and liver weight over body weight ratio. *$p < 0.05$.

(C) Representative H&E and IHC images of PRMT6 and p-ERK1/2 expression of liver tissues harvested from WT or *PRMT6*$^{-/-}$ mice treated with DEN+CCL_4. Scale bar, 100 μm (inset, 20 μm).

(D) Western blot analysis for expression of PRMT6, CD133, NANOG, SOX2, and phosphorylated and total ERK1/2 in non-tumor liver and HCC organoids with PRMT6 stably suppressed or overexpressed, respectively.

(E) Percentage of viable cells in non-tumor liver organoids with PRMT6 suppressed, compared with controls, following 5-flurouracil, cisplatin, and sorafenib treatment. *$p < 0.05$, **$p < 0.01$, and ***$p < 0.001$.

(F) Representative images and quantification of number of cells that migrated, invaded, and formed oncospheres in HCC organoids with PRMT6 overexpressed compared with controls. Scale bar, 100 μm. *$p < 0.05$, **$p < 0.01$, and ***$p < 0.001$.

EV, empty vector control; NT, non-tumor liver; NTC, non-target control; OE, overexpression; T, tumor/HCC. Data are representative of two or more independent experiments. Bars and error represent mean ± SD of replicate measurements.

(Figure 6E). The observation that binding between RAS and CRAF with R100K mutation was not affected by shPRMT6 also confirmed the importance of R100 residue methylation (Figure 6F). To show that PRMT6-mediated methylation regulates RAS/RAF binding, GST-CRAF with or without *in vitro* methylation was subsequently incubated with MBP-RAS for RAS binding assay. Upon PRMT6 *in vitro* methylation, RAS binding affinity was diminished in CRAF wild-type (WT) but not in CRAF R100K mutant (Figure 6G).

Loss of PRMT6 Expression Aggravates Liver Tumorigenesis in a DEN+CCL_4 HCC-Induced PRMT6 Knockout Mouse Model

Next, we extended our studies with PRMT6 knockout (*PRMT6*$^{-/-}$) mice (Neault et al., 2012). WT C57BL/6J and *PRMT6*$^{-/-}$ mice were subjected to DEN+CCl_4 treatment, for induction of a fibrosis/inflammation-associated HCC that closely mimics the disease in human. *PRMT6*$^{-/-}$ mice developed bigger HCC tumors than WT mice and a trend toward higher liver over body weight in *PRMT6*$^{-/-}$ mice (Figures 7A and 7B). H&E staining revealed larger areas of tumors in *PRMT6*$^{-/-}$ mice compared with controls, while IHC also showed absence of PRMT6, concomitant with stronger expression of pERK1/2 in the *PRMT6*$^{-/-}$ mice compared with WT mice (Figure 7C).

PRMT6-Dependent CRAF/ERK Signaling Regulates HCC Stemness as Demonstrated in Patient-Derived Non-tumor Liver and HCC Organoids

To examine whether our hypothesis of a PRMT6-dependent CRAF/ERK signaling regulation of HCC cells could be further

extended in a setting that more closely mimics the real clinical situation, we established non-tumor liver and HCC patient-derived three-dimensional (3D) organoids, with or without PRMT6 stably altered (Figure 7D). Note that our organoids have been thoroughly characterized at both molecular and phenotypic levels, with comparison made against the original non-tumor liver and HCC tissue samples (unpublished data). Knockdown of PRMT6 in non-tumor liver organoids significantly enhanced the abilities of the cells to resist both chemo- and molecular-targeted drugs, while overexpression of PRMT6 in HCC organoids attenuated the cells ability to migrate, invade, and form oncospheres (Figures 7E and 7F). Consistently, alteration in expression of CD133, NANOG, SOX2, and p-ERK1/2 was also observed (Figure 7D).

DISCUSSION

Arginine methylation is a post-translational modification as common as phosphorylation and ubiquitination (Larsen et al., 2016). The methylation of arginine residues is catalyzed primarily by PRMT enzymes, which includes PRMT6. Previous studies found PRMT6 to be predominantly nuclear and methylates arginine- and glycine-rich (RGG/RG) motifs, though it has also been shown to methylate arginines neighboring charged residues, as observed with HIV Tat (Boulanger et al., 2005). PRMT6-mediated methylation is generally associated with transcriptional repression by generating H3R2me2a (Guccione et al., 2007; Iberg et al., 2008; Hyllus et al., 2007; Di Lorenzo et al., 2014), although it has also been reported that PRMT6 functions as a co-activator of nuclear receptors (Harrison et al., 2010). PRMT6-mediated histone methylation also regulates poised chromatin to maintain the balance between pluripotency and differentiation (Lee et al., 2012). In the normal liver, PRMT6 promotes fasting-induced transcriptional activation of gluconeogenesis involving CRTC2 (Han et al., 2014). Earlier studies have suggested the regulatory function of PRMT6 in cellular proliferation, senescence, and cell cycle progression (Kleinschmidt et al., 2012; Phalke et al., 2012; Stein et al., 2012), while one very recent study reported on the role of PRMT6 in regulating DNA methylation and contributing to global DNA hypomethylation in cancers of the breast, prostate, colon, lung, nerve, and bone (Veland et al., 2017). Yet the disease-associated expression and function of PRMT6 in HCC have remained unclear. Our present study finds PRMT6 to play a critical role in negatively regulating the maintenance of stemness feature of HCC cells. It is interesting to also note that, consistent with the study by Veland et al. (2017), our pilot data also suggest that arginine methyltransferase activity of PRMT6 results in DNA hypomethylation in HCC cells, as evident by 5mc immunofluorescence staining. Specifically, global DNA hypomethylation was observed in cells overexpressing WT PRMT6 but not the catalytic inactive PRMT6 mutant (data not shown). However, whether this observed methylation change is dependent on H3R2me2a remains to be elucidated.

The upstream regulator of PRMT6 has not been defined. PRMT6 lies on chromosome 1p13.3, which has previously been reported to be frequently detected in HCC (Guan et al., 2000). Thus, we also did some preliminary analysis on data extracted from TCGA Liver Hepatocellular Carcinoma (LIHC) to examine if gene copy number loss or deletion contributes to the frequent downregulation of PRMT6 in HCC. We found PRMT6 gene copy number loss or deletion to be detected in 23.5% of 370 HCC samples and that the loss was positively correlated with decreased PRMT6 mRNA expression (data not shown). In addition, we also identified a CpG island in the promoter region of PRMT6 and also carried out pilot studies to test if 5-aza-2′-deoxycytidine (5-aza) and trichostatin A (TSA) combination treatment would lead to re-expression of PRMT6 in low-PRMT6-expressing HCC cells. Treatment with 5-aza and TSA resulted in only a slight 2-fold to 3-fold re-expression of PRMT6 (data not shown). Our data on the underlying mechanisms contributing to PRMT6 downregulation in HCC remain inconclusive, and further study is warranted. Whether PRMT6 is regulated by microRNAs (miRNAs) or other regulatory proteins can also be further explored.

PRMT6-mediated H3R2me2a of promoter DNA leads to epigenetic silencing of transcription of the cell cycle inhibitor *p21* as well as the angiogenic inhibitor *TSP1* (Phalke et al., 2012; Michaud-Levesque and Richard, 2009; Nakakido et al., 2015; Kim et al., 2013). It remains to be elucidated whether PRMT6 act as a chromatin modifier in HCC. Our pilot data are at the moment inconclusive, as evidenced by enhanced methylation at the promoter regions of p21, p27, and p57 by H3R2me2a, despite inconsistent p21, p27, and p57 expression change and H3R2me2a expression being unaltered when PRMT6 is modulated (Figure S4). But more interestingly, we observed a predominant cytoplasmic localization of PRMT6 in normal liver and HCC cells, rather than its well-recognized nuclear localization. This observation was validated with two PRMT6 antibodies, including one that is validated by the Human Protein Atlas. Why PRMT6 is predominantly localized in the cytoplasm of liver and HCC cells remains to be answered, but in the past, a number of PRMTs, such as PRMT1 and PRMT5, have also been found to be capable of shuttling between the nucleus and cytoplasm (Herrmann et al., 2005; Herrmann and Fackelmayer, 2009; Gu et al., 2012). For instance, presence of nuclear exclusion signals (NESs) is found responsible for the cytoplasmic localization of PRMT5 in prostate pre-malignant and cancer tissues (Gu et al., 2012). It will be interesting to explore whether liver and HCC cells also contain such NES in the PRMT6 protein.

Although non-histone proteins, including GPS2, CRTC2, Tat, HMGA1a, and PRMT6 itself, are known substrates of PRMT6 (Boulanger et al., 2005; Han et al., 2014; Singhroy et al., 2013; Huang et al., 2015), cytoplasmic proteins specifically methylated by PRMT6 have not been reported. Through an integrative approach, adopting both transcriptome and protein-protein interaction studies, CRAF was identified as one of the cytoplasmic interacting partners of PRMT6. We went on to validate CRAF as a functional substrate of PRMT6 and identified R100 as the specific arginine residue on CRAF targeted by PRMT6. Methylation of CRAF on arginine 100 in the RBD would result in its altered RAS binding potential and thus modulation of the downstream MEK/ERK signaling cascade. Collectively, we found PRMT6 downregulation in HCC to mediate cancer stemness properties via decreased interaction with CRAF and thus reduced methylation on CRAF arginine 100, thereby resulting

in its altered RAS binding potential and subsequent activation of downstream MEK/ERK signaling.

Targeting MEK/ERK signaling and *in vivo* target gene activation of PRMT6 expression in HCC represents a promising anti-cancer stemness therapeutic strategy. In fact, there are a number of MEK/ERK inhibitors available on the market that are either approved for use in patients or under clinical evaluation, including the U.S. Food and Drug Administration (FDA)-approved MEK inhibitors trametinib (GSK1120212) and cobimetinib (GDC-0973, XL518) and MEK/ERK inhibitors in clinical trials, including binimetinib (MEK162), selumetinib, PD-325901, SCH772984, and others. There are now ample data to show that patients respond only partially to single-drug treatments against the MEK/ERK pathways and that MEK/ERK inhibitors would be best if given in combination with other drugs, instead of as a single agent. Our present study revealed that the downregulation of PRMT6 in HCC cells might subject cells to confer cancer and stemness features by activation of MEK/ERK signaling, thus promoting tumor-initiating and therapy resistance in HCC. These results suggest that it may be therapeutically relevant to consider methods to enhance PRMT6 expression in HCC, in combination with use of MEK/ERK inhibitors. In a recent study, Liao et al. (2017) elegantly reported a robust system for *in vivo* activation of endogenous target genes through *trans*-epigenetic remodeling. The system relies on recruitment of Cas9 and transcriptional activation complexes to target loci by modified single-guide RNAs; and as a proof of concept, they used the technology to treat mouse models of diabetes, muscular dystrophy, and acute kidney disease (Liao et al., 2017). This tool can be considered for use in PRMT6 gene activation *in vivo* in HCC patients and as a combination treatment along with use of MEK/ERK inhibitors for anti-cancer stemness targeting in HCC.

STAR★METHODS

Detailed methods are provided in the online version of this paper and include the following:

- KEY RESOURCES TABLE
- CONTACT FOR REAGENTS AND RESOURCE SHARING
- EXPERIMENTAL MODEL AND SUBJECT DETAILS
  - Cell lines and organoid cultures
  - Archived patient samples
  - Animal studies
- METHODS DETAILS
  - Reagents, kits and plasmids
  - Flow cytometry and cell sorting
  - Gene expression profiling
  - Agilent microarray profiling
  - Quantitative real-time PCR
  - Western blot and co-immunoprecipitation
  - Lentiviral production and cell transduction
  - CRISPR/Cas9 knockout
  - Immunohistochemistry
  - Immunofluorescence
  - Oncosphere-forming and self-renewal assay
  - Cell motility and invasion assays
  - Annexin V apoptosis assay
  - Cell viability assay
  - Tandem affinity purification – mass spectrometry
  - Methylation assays
  - Liquid chromatography–mass spectrometry analysis
  - *In vitro* RAS binding assay
  - ChIP-qPCR
- QUANTIFICATION AND STATISTICAL ANALYSIS
- DATA AND SOFTWARE AVAILABILITY

SUPPLEMENTAL INFORMATION

Supplemental Information includes seven figures and seven tables and can be found with this article online at https://doi.org/10.1016/j.celrep.2018.09.053.

ACKNOWLEDGMENTS

This project is supported in part by grants from the Research Grants Council of Hong Kong – General Research Fund (17143516), Collaborative Research Fund (C7027-14G), and Theme Based Research Scheme (T12-710/16-R), as well as an Innovation Award from the Croucher Foundation. We thank the Faculty Core Facility and Proteomics & Metabolomics Core Facility (The University of Hong Kong) for providing and maintaining the equipment and technical support needed for flow cytometry analysis and cell sorting, animal imaging, confocal microscopy, and mass spectrometry.

AUTHOR CONTRIBUTIONS

L.H.C. and S.M. conceived the project. L.H.C., L.Z., K.Y.N., and T.L.W. performed the research and analyzed and interpreted the data. T.K.L., X.Y.G., Y.P.C., and M.S.Y.H. provided plasmids and reagents. T.K.L. provided critical scientific input. R.S. performed mass spectrometry experiments. J.H.L. helped with organoid experiments. Y.F.Y., D.X., C.M.L., and K.M. obtained patient consent and provided the clinical samples and patient information. B.A., H.C., H.H.Y., and S.Y.L. provided expertise and reagents for liver organoid culture. S.R. provided PRMT6 WT and catalytically inactive mutant plasmids, PRMT6 knockout mice, as well as expertise on PRMT studies. M.S.Y.H. provided expertise and reagents for tandem affinity purification/mass spectrometry studies and assisted in data analysis. L.H.C., L.Z., K.Y.N., T.L.W., and S.M. wrote the manuscript. S.M. analyzed and interpreted the data, supervised the project, and provided funding for this study.

DECLARATION OF INTERESTS

The authors declare no competing interests.

Received: April 26, 2018
Revised: July 26, 2018
Accepted: September 16, 2018
Published: October 16, 2018

REFERENCES

Almeida-Rios, D., Graça, I., Vieira, F.Q., Ramalho-Carvalho, J., Pereira-Silva, E., Martins, A.T., Oliveira, J., Gonçalves, C.S., Costa, B.M., Henrique, R., and Jerónimo, C. (2016). Histone methyltransferase PRMT6 plays an oncogenic role of in prostate cancer. Oncotarget *7*, 53018–53028.

Bedford, M.T., and Clarke, S.G. (2009). Protein arginine methylation in mammals: who, what, and why. Mol. Cell *33*, 1–13.

Blanc, R.S., and Richard, S. (2017). Arginine methylation: the coming of age. Mol. Cell *65*, 8–24.

Boulanger, M.C., Liang, C., Russell, R.S., Lin, R., Bedford, M.T., Wainberg, M.A., and Richard, S. (2005). Methylation of Tat by PRMT6 regulates human immunodeficiency virus type 1 gene expression. J. Virol. *79*, 124–131.

Di Lorenzo, A., Yang, Y., Macaluso, M., and Bedford, M.T. (2014). A gain-of-function mouse model identifies PRMT6 as a NF-κB coactivator. Nucleic Acids Res. *42*, 8297–8309.

Feng, W., Guo, Y., Huang, J., Deng, Y., Zang, J., and Huen, M.S. (2016). TRAIP regulates replication fork recovery and progression via PCNA. Cell Discov. *2*, 16016.

Frankel, A., Yadav, N., Lee, J., Branscombe, T.L., Clarke, S., and Bedford, M.T. (2002). The novel human protein arginine N-methyltransferase PRMT6 is a nuclear enzyme displaying unique substrate specificity. J. Biol. Chem. *277*, 3537–3543.

Gu, Z., Li, Y., Lee, P., Liu, T., Wan, C., and Wang, Z. (2012). Protein arginine methyltransferase 5 functions in opposite ways in the cytoplasm and nucleus of prostate cancer cells. PLoS ONE *7*, e44033.

Guan, X.Y., Fang, Y., Sham, J.S., Kwong, D.L., Zhang, Y., Liang, Q., Li, H., Zhou, H., and Trent, J.M. (2000). Recurrent chromosome alterations in hepatocellular carcinoma detected by comparative genomic hybridization. Genes Chromosomes Cancer *29*, 110–116.

Guccione, E., Bassi, C., Casadio, F., Martinato, F., Cesaroni, M., Schuchlautz, H., Lüscher, B., and Amati, B. (2007). Methylation of histone H3R2 by PRMT6 and H3K4 by an MLL complex are mutually exclusive. Nature *449*, 933–937.

Han, H.S., Jung, C.Y., Yoon, Y.S., Choi, S., Choi, D., Kang, G., Park, K.G., Kim, S.T., and Koo, S.H. (2014). Arginine methylation of CRTC2 is critical in the transcriptional control of hepatic glucose metabolism. Sci. Signal. *7*, ra19.

Harrison, M.J., Tang, Y.H., and Dowhan, D.H. (2010). Protein arginine methyltransferase 6 regulates multiple aspects of gene expression. Nucleic Acids Res. *38*, 2201–2216.

Herrmann, F., and Fackelmayer, F.O. (2009). Nucleo-cytoplasmic shuttling of protein arginine methyltransferase 1 (PRMT1) requires enzymatic activity. Genes Cells *14*, 309–317.

Herrmann, F., Lee, J., Bedford, M.T., and Fackelmayer, F.O. (2005). Dynamics of human protein arginine methyltransferase 1(PRMT1) *in vivo*. J. Biol. Chem. *280*, 38005–38010.

Huang, J., Cardamone, M.D., Johnson, H.E., Neault, M., Chan, M., Floyd, Z.E., Mallette, F.A., and Perissi, V. (2015). Exchange factor TBL1 and arginine methyltransferase PRMT6 cooperate in protecting G protein pathway suppressor 2 (GPS2) from proteasomal degradation. J. Biol. Chem. *290*, 19044–19054.

Huch, M., Gehart, H., van Boxtel, R., Hamer, K., Blokzijl, F., Verstegen, M.M., Ellis, E., van Wenum, M., Fuchs, S.A., de Ligt, J., et al. (2015). Long-term culture of genome-stable bipotent stem cells from adult human liver. Cell *160*, 299–312.

Hyllus, D., Stein, C., Schnabel, K., Schiltz, E., Imhof, A., Dou, Y., Hsieh, J., and Bauer, U.M. (2007). PRMT6-mediated methylation of R2 in histone H3 antagonizes H3 K4 trimethylation. Genes Dev. *21*, 3369–3380.

Iberg, A.N., Espejo, A., Cheng, D., Kim, D., Michaud-Levesque, J., Richard, S., and Bedford, M.T. (2008). Arginine methylation of the histone H3 tail impedes effector binding. J. Biol. Chem. *283*, 3006–3010.

Ito, Y., Sasaki, Y., Horimoto, M., Wada, S., Tanaka, Y., Kasahara, A., Ueki, T., Hirano, T., Yamamoto, H., Fujimoto, J., et al. (1998). Activation of mitogen-activated protein kinases/extracellular signal-regulated kinases in human hepatocellular carcinoma. Hepatology *27*, 951–958.

Kim, N.H., Kim, S.N., Seo, D.W., Han, J.W., and Kim, Y.K. (2013). PRMT6 overexpression upregulates TSP-1 and downregulates MMPs: its implication in motility and invasion. Biochem. Biophys. Res. Commun. *432*, 60–65.

Kleinschmidt, M.A., de Graaf, P., van Teeffelen, H.A., and Timmers, H.T. (2012). Cell cycle regulation by the PRMT6 arginine methyltransferase through repression of cyclin-dependent kinase inhibitors. PLoS ONE *7*, e41446.

Larsen, S.C., Sylvestersen, K.B., Mund, A., Lyon, D., Mullari, M., Madsen, M.V., Daniel, J.A., Jensen, L.J., and Nielsen, M.L. (2016). Proteome-wide analysis of arginine monomethylation reveals widespread occurrence in human cells. Sci. Signal. *9*, rs9.

Lavoie, H., and Therrien, M. (2015). Regulation of RAF protein kinases in ERK signalling. Nat. Rev. Mol. Cell Biol. *16*, 281–298.

Lee, Y.H., Ma, H., Tan, T.Z., Ng, S.S., Soong, R., Mori, S., Fu, X.Y., Zernicka-Goetz, M., and Wu, Q. (2012). Protein arginine methyltransferase 6 regulates embryonic stem cell identity. Stem Cells Dev. *21*, 2613–2622.

Liao, H.K., Hatanaka, F., Araoka, T., Reddy, P., Wu, M.Z., Sui, Y., Yamauchi, T., Sakurai, M., O'Keefe, D.D., Núñez-Delicado, E., et al. (2017). *In vivo* target gene activation via CRISPR/Cas9-mediated *trans*-epigenetic modulation. Cell *171*, 1495–1507.e15.

Limm, K., Ott, C., Wallner, S., Mueller, D.W., Oefner, P., Hellerbrand, C., and Bosserhoff, A.K. (2013). Deregulation of protein methylation in melanoma. Eur. J. Cancer *49*, 1305–1313.

Michaud-Levesque, J., and Richard, S. (2009). Thrombospondin-1 is a transcriptional repression target of PRMT6. J. Biol. Chem. *284*, 21338–21346.

Nakakido, M., Deng, Z., Suzuki, T., Dohmae, N., Nakamura, Y., and Hamamoto, R. (2015). PRMT6 increases cytoplasmic localization of p21CDKN1A in cancer cells through arginine methylation and makes more resistant to cytotoxic agents. Oncotarget *6*, 30957–30967.

Neault, M., Mallette, F.A., Vogel, G., Michaud-Levesque, J., and Richard, S. (2012). Ablation of PRMT6 reveals a role as a negative transcriptional regulator of the p53 tumor suppressor. Nucleic Acids Res. *40*, 9513–9521.

Phalke, S., Mzoughi, S., Bezzi, M., Jennifer, N., Mok, W.C., Low, D.H., Thike, A.A., Kuznetsov, V.A., Tan, P.H., Voorhoeve, P.M., and Guccione, E. (2012). p53-independent regulation of p21Waf1/Cip1 expression and senescence by PRMT6. Nucleic Acids Res. *40*, 9534–9542.

Singhroy, D.N., Mesplède, T., Sabbah, A., Quashie, P.K., Falgueyret, J.P., and Wainberg, M.A. (2013). Automethylation of protein arginine methyltransferase 6 (PRMT6) regulates its stability and its anti-HIV-1 activity. Retrovirology *10*, 73.

Stein, C., Riedl, S., Rüthnick, D., Nötzold, R.R., and Bauer, U.M. (2012). The arginine methyltransferase PRMT6 regulates cell proliferation and senescence through transcriptional repression of tumor suppressor genes. Nucleic Acids Res. *40*, 9522–9533.

Uehara, T., Pogribny, I.P., and Rusyn, I. (2014). The DEN and CCl4-induced mouse model of fibrosis and inflammation-associated hepatocellular carcinoma. Curr. Protocols Pharmacol. *66*, 1–10.

Veland, N., Hardikar, S., Zhong, Y., Gayatri, S., Dan, J., Strahl, B.D., Rothbart, S.B., Bedford, M.T., and Chen, T. (2017). The arginine methyltransferase PRMT6 regulates DNA methylation and contributes to global DNA hypomethylation in cancer. Cell Rep. *21*, 3390–3397.

Visvader, J.E., and Lindeman, G.J. (2012). Cancer stem cells: current status and evolving complexities. Cell Stem Cell *10*, 717–728.

Yamashita, T., and Wang, X.W. (2013). Cancer stem cells in the development of liver cancer. J. Clin. Invest. *123*, 1911–1918.

Yoshimatsu, M., Toyokawa, G., Hayami, S., Unoki, M., Tsunoda, T., Field, H.I., Kelly, J.D., Neal, D.E., Maehara, Y., Ponder, B.A., et al. (2011). Dysregulation of PRMT1 and PRMT6, Type I arginine methyltransferases, is involved in various types of human cancers. Int. J. Cancer *128*, 562–573.

STAR★METHODS

KEY RESOURCES TABLE

REAGENT or RESOURCE	SOURCE	IDENTIFIER
Antibodies		
PE-conjugated anti-human CD133 (FACS)	Miltenyi Biotec	Cat No. 130-080-901; RRID: AB_244348
FITC-conjugated anti-human CD24 (FACS)	BD Biosciences	Cat No. 555427; RRID: AB_395821
FITC-conjugated anti-human CD90 (FACS)	Miltenyi Biotec	Cat No. 130-097-930; RRID: AB_2660947
Anti-human/mouse PRMT6 (WB, IHC and IF)	Abcam	Cat No. ab47244; RRID: AB_2284473
Anti-human CD133 (WB)	Miltenyi Biotec	Cat No. 130-092-395; RRID: AB_615061
Anti-human ADMA	Cell Signaling Technology	Cat No. 13522; RRID: AB_2665370
Anti-human SOX2	Abcam	Cat No. ab97959; RRID: AB_2341193
Anti-human NANOG	Cell Signaling Technology	Cat No. 3580; RRID: AB_2150399
Anti-human H3R2me2a	Millipore	Cat No. 07-585; RRID: AB_310733
Anti-human FLAG	Sigma-Aldrich	Cat No. F3165; RRID: AB_259529
Anti-human p-CRAF (S338)	Cell Signaling Technology	Cat No. 9427; RRID: AB_2067317
Anti-human CRAF	Cell Signaling Technology	Cat No. 12552; RRID: AB_2728706
Anti-human ARAF	Cell Signaling Technology	Cat No. 4432; RRID: AB_330813
Anti-human BRAF	Cell Signaling Technology	Cat No. 9433; RRID: AB_2259354
Anti-human p-ERK1/2	Cell Signaling Technology	Cat No. 9101; RRID: AB_331646
Anti-human ERK1/2 (for WB and ERK kinase assay)	Cell Signaling Technology	Cat No. 9102; RRID: AB_330744
Anti-human p-MEK1/2 (S217/221)	Cell Signaling Technology	Cat No. 9154; RRID: AB_2138017
Anti-human MEK1/2	Cell Signaling Technology	Cat No. 9122; RRID: AB_823567
Anti-human RAS	Calbiochem	Cat No. OP01L; RRID: AB_565094
Anti-human Histone H3	Abcam	Cat No. ab24834; RRID: AB_470335
Anti-human β-actin	Sigma-Aldrich	Cat No. A5316; RRID: AB_476743
Anti-human PRMT6 (for Co-IP)	Bethyl Laboratories	Cat No. A300-928A; RRID: AB_661910
Rabbit IgG control (for Co-IP)	Santa Cruz	Cat No. sc-2027; RRID: AB_737197
Anti-human PRMT6 (for IHC and IF)	Atlas Antibodies	Cat No. HPA059424; RRID: AB_2684012
Anti-human SOX2 (for IHC)	R&D Systems	Cat No. MAB2018; RRID: AB_358009
Anti-human p-ERK1/2 (for IHC)	Abcam	Cat No. ab50011; RRID: AB_1603684
Anti-human H3 (asymmetric di methyl R2)	Abcam	Cat No. ab175007
Anti-human CRAF (for CRAF kinase assay)	Millipore	Cat No. 07-396; RRID: AB_310580
Anti-human p53	Cell Signaling Technology	Cat No. 9282; RRID: AB_10693944
Bacterial and Virus Strains		
BL21(DE3) competent *E.coli*	New England Biolabs	Cat No. C2527I
DH5α competent *E.coli*	Invitrogen	Cat No. 18265017
Biological Samples		
HCC and distal adjacent non-tumor liver tissues	Queen Mary Hospital (Hong Kong)	N/A
Human and distal adjacent non-tumor liver tissues	Sun Yat-Sen University Cancer Center (China)	N/A
Chemicals, Peptides, and Recombinant Proteins		
MEK inhibitor U0126	Cell Signaling Technology	Cat No. 9903
Unmodified CRAF R100 peptide (CAVFRLLHE)	GenScript	N/A
Modified CRAF R100K peptide (CAVFKLLHE)	GenScript	N/A
Critical Commercial Assays		
ERK kinase assay (KinaseSTAR JNK assay kit)	BioVision	Cat No. K431-40
CRAF kinase assay	Millipore (Upstate)	Cat No. 17-360
PrimeSTAR GXL kit	Takara	Cat No. R050B

(*Continued on next page*)

Continued

REAGENT or RESOURCE	SOURCE	IDENTIFIER
PrimeScript RT Master Mix	Takara	Cat No. RR036A
EvaGreen qPCR Master Mix	ABM	Cat No. MasterMix-S-XL
Millicell Hanging Inserts (for migration assay)	Millipore	Cat No. PIEP12R48
Biocoat Matrigel Invasion Chambers	BD Biosciences	Cat No. 354480
Annexin V-FLUOS Staining Kit	Roche	Cat No. 11828681001
CellTiter-Glo Assay	Promega	Cat No. G7570
Magna ChIP G – Chromatin Immunoprecipitation Kit	Millipore	Cat No. 17-611
Deposited Data		
cDNA microarray (NTC control versus PRMT6 KD)	GEO, NCBI	GSE97931
Experimental Models: Cell Lines		
Human HCC cell line SNU182	ATCC	ATCC CRL-2235
Human HCC cell line HepG2	ATCC	ATCC HB8065
Human HCC cell line PLC8024	Institute of Virology, Chinese Academy of Sciences (China)	N/A
Human HCC cell line BEL7402	Shanghai Institute of Cell Biology, Chinese Academy of Sciences (China)	N/A
Human HCC cell line Huh7	JCRB Cell Bank	JCRB0403
Human HCC cell line MHCC97L	Liver Cancer Institute, Fudan University (China)	N/A
Human 293FT	Invitrogen	R70007
Human 293T	ATCC	ATCC CRL-3216
Human 293T/17	ATCC	ATCC CRL-11268
Experimental Models: Organisms/Strains		
PRMT6$^{-/-}$ mice	Provided by Dr. Stèphane Richard (McGill University) (Neault et al., 2012)	N/A
C57BL/6J mice	Laboratory Animal Unit, University of Hong Kong	N/A
BALB/C nude mice	Laboratory Animal Unit, University of Hong Kong	N/A
NOD/SCID mice	Laboratory Animal Unit, University of Hong Kong	N/A
Oligonucleotides		
Primers for sub-cloning of WT PRMT6 and catalytically inactive PRMT6 mutant into pDONR201	Table S7	N/A
Primers for sub-cloning of FL and truncated mutants of CRAF into pDONR201	Table S7	N/A
Primers for sub-cloning of RAS into pDONR201	Table S7	N/A
Primers for construction of site-directed mutants of CRAF (R89K and R100K)	Table S7	N/A
Primers for cloning of PRMT6 knockouts	Table S7	N/A
PRMT6 qPCR primers	Table S7	N/A
p21 qPCR primers	Table S7	N/A
p27 qPCR primers	Table S7	N/A
p57 qPCR primers	Table S7	N/A
β-actin qPCR primers	Table S7	N/A
Recombinant DNA		
WT PRMT6 and catalytically inactive PRMT6 mutant	Provided by Dr. Stèphane Richard (McGill University) (Neault et al., 2012)	N/A

(*Continued on next page*)

Continued

REAGENT or RESOURCE	SOURCE	IDENTIFIER
pDONR201	Invitrogen	N/A
CMV-SFB	Provided by Dr. Michael Huen (University of Hong Kong)	N/A
HA-FLAG	Provided by Dr. Michael Huen (University of Hong Kong)	N/A
pMH-MBP	Provided by Dr. Michael Huen (University of Hong Kong)	N/A
pEZ-Lv199	Genecopoeia	N/A
PRMT6 overexpression in pEZ-Lv199	Genecopoeia	N/A
Glutathione S-transferase (GST)-tag containing pGEX4t1 vector	GE Healthcare Life Sciences	Cat No. 28954549
PRMT6-specific shRNA expression vector - shRNA clone ID TRCN0000299933 (CCGGCACGGACGTTTCAGGAGA GATCTCGAGATCTCTCCTGAAACGTCCGTGTTTTTG)	Sigma-Aldrich	N/A
PRMT6-specific shRNA expression vector - shRNA clone ID TRCN0000299956 (CCGGCACCGGCATTCTGAGCAT CTTCTCGAGAAGATGCTCAGAATGCCGGTGTTTTTG)	Sigma-Aldrich	N/A
ERK1-specific shRNA expression vector – shRNA clone (CCGGCTATACCAAGTCCATCGACATCTCGAGATGTC GATGGACTTGGTATAGTTTTTG)	Sigma-Aldrich	N/A
ERK2-specific shRNA expression vector shRNA clone (CCGGGACATTATTCGAGCACCAACCCTCGAGGGTT GGTGCTCG AATAATGTCTTTTTG)	Sigma-Aldrich	N/A
Non-target scrambled control (NTC) (CCGGCAACAAGA TGAAGAGCACAACTCGAGTTGGTGCTCTTCATC TTGTTGTTTTT)	Sigma-Aldrich	N/A
LentiCRISPR-v2 plasmid	Addgene	52961
Software and Algorithms		
Gene Set Enrichment Analysis (GSEA)	Broad Institute	http://software.broadinstitute.org/gsea/index.jsp
Ingenuity Pathway Analysis (IPA)	QIAGEN	https://www.qiagenbioinformatics.com/products/ingenuity-pathway-analysis/
FlowJo	TreeStar	https://www.flowjo.com/
GraphPad Prism 5.0	GraphPad	https://www.graphpad.com/scientific-software/prism/
SPSS 21.0	IBM	N/A
Extreme Limiting Dilution Analysis (ELDA)	N/A	PMID 19567251
PEAKS DB software	Bioinformatics Solutions Ltd.	PMID 22186715

CONTACT FOR REAGENTS AND RESOURCE SHARING

Further information and requests for resources and reagents should be directed to and will be fulfilled by the Lead Contact, Stephanie Ma (stefma@hku.hk).

EXPERIMENTAL MODEL AND SUBJECT DETAILS

Cell lines and organoid cultures

HCC cell lines SNU182 and HepG2 were purchased from American Type Culture Collect (ATCC). HCC cell lines PLC8024 and BEL7402 was obtained from Institute of Virology and Shanghai Institute of Cell Biology, respectively, of the Chinese Academy of Sciences, Beijing, China. HCC cell line, Huh7, was provided by JCRB Cell Bank (Japan). MHCC97L cells were obtained from Liver Cancer Institute, Fudan University, China. 293T and 293T/17 cells were purchased from ATCC; while 293FT was purchased from

Invitrogen. Cell lines used in this study were regularly authenticated by morphological observation and tested for absence of Mycoplasma contamination. HCC and distal adjacent non-tumor liver tissues were obtained from patients undergoing hepatectomy or liver transplantation at Queen Mary Hospital, Hong Kong. Informed consent was obtained from all patients before the collection of liver specimens. Specimen collection and all experiments were approved by the Institutional Review Board of the University of Hong Kong / Hospital Authority Hong Kong West Cluster. Samples were collected from patients who had not received any previous local or systemic treatment prior to operation. For organoid cultures, cells were isolated and cultured according to previously reported protocol (Huch et al., 2015). Liver cells were isolated from human liver biopsies (0.5–1cm^3) by collagenase-accutase digestion. The different fractions were mixed and washed with cold Advanced DMEM/F12 and spun at 300–400 × *g* for 5 min. The cell pellet was mixed with Matrigel (BD Biosciences) and 3,000–10,000 cells were seeded per well in a 24-well/plate. After Matrigel had solidified, culture medium was added. Culture media was based on AdDMEM/F12 (Invitrogen) supplemented with 1% N2 and 1% B27 (both from GIBCO), 1.25mM N-Acetylcysteine (Sigma), 10nM gastrin (Sigma), and the growth factors: 50ng/ml EGF (Peprotech), 10% RSPO1 conditioned media (homemade), 100ng/ml FGF10 (Peprotech), 25ng/ml HGF (Peprotech), 10mM Nicotinamide (Sigma), 5μM A83.01 (Tocris), and 10μM FSK (Tocris). For the establishment of the culture, the first 3 days after isolation, the medium was supplemented with 25ng/ml Noggin (Peprotech), 30% Wnt CM (homemade prepared), and 10μM (Y27632, Sigma Aldrich). Then, the medium was changed into a medium without Noggin, Wnt or Y27632. After 10–14 days, organoids were removed from the Matrigel, mechanically dissociated into small fragments, and transferred to fresh matrix. Passage was performed in a 1:4–1:8 split ratio once every 7–10 days for at least 6 months. HCC and distant adjacent non-tumor liver tissues used for organoid established were also obtained from patients undergoing hepatectomy or liver transplantation at Queen Mary Hospital, Hong Kong, with informed consent obtained from all patients and protocol approved by ethics committee as stated above.

Archived patient samples

Formalin-fixed paraffin-embedded primary human HCC and adjacent non-tumor liver tissue samples were obtained from HCC patients who underwent surgical resection at the Sun Yat-Sen University Cancer Centre in Guangzhou, China. Informed consent was obtained from all patients before the collection of liver specimens. Specimen collection and all experiments were approved by the Institutional Review Board of Sun Yat-Sen University. Tissue samples were collected from patients who had not received any previous local or systemic treatment prior to operation.

Animal studies

The study protocol was approved by and performed in accordance with the Committee of the Use of Live Animals in Teaching and Research at The University of Hong Kong. PRMT6$^{-/-}$ mice were provided by Stéphane Richard (Neault et al., 2012). PRMT6$^{-/-}$ mice were viable, fertile and did not display any overt phenotype. WT C57BL/6J and PRMT6$^{-/-}$ mice were treated with N-nitrosodiethylamine (DEN, intraperitoneal, 1mg/kg) at the age of 14 days. Starting at 8 weeks of age, carbon tetrachloride (CCl_4, intraperitoneal, 0.2ml/kg) was administered twice weekly for an additional 14 weeks (Uehara et al., 2014). Body weight, liver weight, number and size of tumors were measured at end point. Livers were harvested for histological analysis. Tumorigenicity was determined by subcutaneous injection into the flank of 4-to-5 week old male BALB/C nude or NOD/SCID mice. Tumor-initiating and self-renewal abilities were investigated by limiting dilution and serial transplantation assays. 4-to-6 week old male NOD/SCID mice were injected subcutaneously with either 5,000 or 10,000 cells. Tumor incidence and tumor latency were recorded. Tumor-initiating frequency was calculated using the Extreme Limiting Dilution Analysis (ELDA) software. Established xenografts were harvested and dissociated for subsequence passage to secondary mouse recipients. After tumors were detected, tumor sizes were measured every 3 days by calipers and tumor volumes were calculated as volume (cm^3) = L x W^2 x 0.5 with L and W representing the largest and smallest diameters, respectively. Tumors formed were harvested for histological analysis. Metastasis was assessed by orthotopically injecting into the liver of 6 week old BALB/C nude mice to observe for lung metastasis. Specifically, luciferase-labeled cells were injected into the left lobes of the livers of BALB/C nude mice. Six weeks after implantation, mice were administered with 100mg/kg D-luciferin via peritoneal injection 5 mins before bioluminescent imaging (IVIS^{TM} 100 Imaging System, Xenogen). Livers were harvested for *ex vivo* imaging and histological analysis. Animals that were injected with tumor cells but showed no sign of tumor burden were generally terminated six months after tumor cell inoculation, and animals were opened up at the injection sites to confirm that there was no tumor development.

METHODS DETAILS

Reagents, kits and plasmids

WT PRMT6 and catalytically inactive PRMT6 mutant (Neault et al., 2012) were provided by Stèphane Richard (McGill University, Canada). MEK inhibitor U0126 was purchased from Cell Signaling Technologies. ERK kinase assay was performed using the KinaseSTAR JNK assay kit (BioVision) where c-Jun was used as a substrate. CRAF kinase assay was purchased from Millipore (Upstate) where MEK1/2 was used as a substrate. WT and catalytically inactive PRMT6 were subcloned into Gateway entry vector pDONR201 (Invitrogen) using the forward primer 5′-GGGGACAAGTTTGTACAAAAAAGCAGGCTCCATGTCGCAGCCCAAGAAAA GAAAGC-3′ and reverse primer 5′-GGGGACCACTTTGTACAAGAAAGCTGGGTCCTAGTCCTCCATGGCAAAGTCTTTG-3′. FL and

the truncated mutants of CRAF were cloned into Gateway vector pDONR201 by the following primers: FL: F (5′-GGGGACAAGTTTG TACAAAAAAGCAGGCTCCATGGAGCACATACAGGGAGCTTGGA-3′), R (5′-GGGGACCACTTTGTACAAGAAAGCTGGGTCCTAG AAGACAGGCAGCCTCGGGGAC-3′); D1 (5′-GGGGACCACTTTGTACAAGAAAGCTGGGTCTTACATGAAGATGATCTGATCTCGG-3′); D2 (5′-GGGGACCACTTTGTACAAGAAAGCTGGGTCTTACTGGGTCCCAGATACTGGTGCC-3′); D3 (5′-GGGGACCACTTTGTA CAAGAAAGCTGGGTCTTAAGACTCTCGCATACGACGCATA-3′); D4 (5′-GGGG-ACCACTTTGTACAAGAAAGCTGGGTCTTAGTTG TGTGTTGTGAGGGGAACA-3′); D5 (5′-GGGG ACCACTTTGTACAAGAAAGCTGGGTCTTAGTCATGCAAGCTCATTCCATTT-3′); D6 (5′-GGGGACAAGT TTGTACAAAAAAGCAGGCTCCATGTGCCTTATGAAAGCACTCAAGG-3′). PCR reactions were performed using the PrimeSTAR GXL kit (Takara). Gateway compatible plasmids including CMV-SFB, HA-FLAG and pMH-MBP were provided by Michael Huen (The University of Hong Kong, China). Recombination steps were accomplished with the use of Gateway and BP Clonase II and LR Clonase II (Invitrogen). WT and catalytic inactive PRMT6 were shuttled into the EZShuttle recombination cloning expression vector pEZ-Lv199 (Genecopoeia) for lentiviral-based stable overexpression. RAS was subcloned into Gateway entry vector pDONR201 (Invitrogen) using forward primer 5′- GGGGACAAGTTTGTACAAAAAAGCAGGCTATGACGGAATATAA GCTGGTGGT-3′ and reverse primer 5′- GGGGACCACTTTGTACAAGAAAGCTGGGTCAGGAGAGCACACACTTGC-3′; and subsequently shuttled into pMH-MBP. The site-directed mutants of CRAF were constructed using the primers: R89K F (5′-CTCAAGG TGAAAGGCCTGCAA-3′), R (5′- TTGCAGGCCTTTCACCTTGAG-3′) and R100K F (5′- GCAGTGTTCAAACTTCTCCAC-3′), R (5′- GTGGAGAAGTTTGAACACTGC-3′) such that arginine-to-lysine conversions were introduced. For *in vitro* methylation assay, WT and site-directed mutants were subcloned into glutathione S-transferase (GST)-tag containing pGEX4t1 vector (Addgene). All DNA expression constructs were confirmed by DNA sequencing.

Flow cytometry and cell sorting

Flow cytometry analysis or flow cytometry cell sorting was conducted using PE-conjugated mouse anti-human CD133 (Miltenyi Biotec), FITC-conjugated mouse anti-human CD24 (BD Biosciences), FITC-conjugated mouse anti-human CD90 (Miltenyi Biotec) and its respective isotype control. Samples were analyzed and sorted on BD FACSCanto II and FACSAria I, respectively (BD Biosciences) with data analyzed by FlowJo (Tree Star Inc.).

Gene expression profiling

Gene expression profiling studies involving non-tumor liver (n = 50) and HCC (n = 371) tissue samples were performed analyzing the expression of PRMT6 transcripts available under Liver Hepatocellular Carcinoma (LIHC) of the TCGA Research Network and analyzed using UCSC Xena Browser.

Agilent microarray profiling

cDNA microarray profiling on Agilent Human Gene Expression Array 8x60K v3 was performed as a service at Macrogen. Pathway enrichment analyses on the differentially expressed genes were conducted using Gene Set Enrichment Analysis (GSEA, Broad Institute) and Ingenuity Pathway Analysis (IPA, QIAGEN) softwares.

Quantitative real-time PCR

Total RNA was extracted using RNA-IsoPlus (Takara) and cDNA was synthesized by PrimeScript RT Master Mix (Takara). qPCR was performed with EvaGreen qPCR Master Mix (ABM) and the following primers PRMT6: F (5′-ACGAGTGCTACTCGGACGTT-3′), R (5′-AGTTCCGAAGGATACCCAGG-3′) and β-ACTIN: F (5′- CATCCACGAAACTACCTTCAACTCC-3′), R (5′- GAGCCGCCGATC CACACG-3′) on an ABI Prism 7900 System (Applied Biosystems) with data analyzed using the ABI SDS v2.3 software (Applied Biosystems). Relative expression differences were calculated using the $2^{-\Delta\Delta Ct}$ method.

Western blot and co-immunoprecipitation

Protein lysates were quantified and resolved on a SDS-PAGE gel, transferred onto a PVDF membrane (Millipore) and immunoblotted with a primary antibody, followed by incubation with a secondary antibody. Antibody signal was detected using an enhanced chemiluminescence system (GE Healthcare). The following antibodies were used: PRMT6 (1:500, Abcam, ab47244) (Phalke et al., 2012), CD133 (1:500, Miltenyi Biotec, 130-092-395), AMDA (1:1000, Cell Signaling, 13522), SOX2 (1:1000, Abcam, ab97959), NANOG (1:1000, Cell Signaling, 3580), H3R2me2a (1:1000, Millipore, 07-585), FLAG (1:5000, Sigma-Aldrich, F3165), p-CRAF (S338) (1:1000, Cell Signaling, 9427), CRAF (1:1000, Cell Signaling, 12552), ARAF (1:1000, Cell Signaling, 4432), BRAF (1:1000, Cell Signaling, 9433), p-ERK1/2 (1:1000, Cell Signaling, 9101), ERK1/2 (1:1000, Cell Signaling, 9102), p-MEK1/2 (S217/221) (1:1000, Cell Signaling, 9154), MEK1/2 (1:1000, Cell Signaling, 9122), RAS (1:500, Calbiochem, OP01L), Histone H3 (1:1000, Abcam, ab24834), p53 (1:1000, Cell Signaling, 9282) and β-ACTIN (1:5000, Sigma-Aldrich, A5316). For Co-IP experiments, cells were lysed by ice-cold NETN buffer (20mM Tris-HCl pH 8.0, 100mM NaCl, 1mM EDTA and 0.5% v/v NP40), and the SFB- or HA-FLAG-tagged proteins were pulled-down by streptavidin bead slurry (Amersham) and anti-FLAG M2 affinity gel (Sigma-Aldrich), respectively. The proteins were precipitated by incubation under 4°C for 3-4 hr with gentle shaking. For endogenous PRMT6 Co-IP experiments, cells were lysed by ice-cold NETN buffer and endogenous PRMT6 was pulled-down by PRMT6 antibody (5 μg/mg lysate, Bethyl Laboratories, A300-928A) and Protein A Sepharose (BioVision). The proteins were precipitated by incubation under 4°C for 16 hr

with gentle shaking. Rabbit IgG (Santa Cruz, sc-2027) was used as control. The protein was eluted by heating at 95°C for 5 mins and mixed with 6x loading buffer for SDS-PAGE and western blot analyses.

Lentiviral production and cell transduction

PRMT6-specific shRNA expression vectors (NM_018137.2) and the scrambled shRNA non-target control (NTC) were purchased from Sigma-Aldrich. Sequences of the two shRNAs directed against PRMT6 are as follows: clone ID TRCN0000299933 (CCGGCACGGACGTTTCAGGAGAGATCTCGAGATCTCTCCTGAAACGTCCGTGTTTTTG) and clone ID TRCN0000299956 (CCGGCACCGGCATTCTGAGCATCTTCTCGAGAAGATGCTCAGAATGCCGGTGTTTTTG). Sequences directed against ERK1 and ERK2 are as follow: (CCGGCTATACCAAGTCCATCGACATCTCGAGATGTCGATGGACTTGGTATAGTTTTTG) and (CCGGGACAT TATTCGAGCACCAACCCTCGAGGGTTGGTGCTCGAATAATGTCTTTTTG), respectively. Sequence of NTC is (CCGGCAACAAGAT GAAGAGCACAACTCGAGTTGGTGCTCTTCATCTTGTTGTTTTT). Sequences were transfected into 293FT cells and packaged using MISSION Lentiviral Packaging Mix (Sigma-Aldrich). PRMT6 lentiviral overexpression or empty vector control plasmids were purchased from Genecopoeia. Sequences were transfected into 293T cells and packaged using Lenti-Pac HIV expression packaging mix (Genecopoeia) or Viral Power packaging mix (Invitrogen). Virus-containing supernatants were collected for subsequent transduction to establish cells with PRMT6 stably repressed or overexpressed. Puromycin or blasticidin were used for cell selection. For transduction of organoids, the same overexpression and knockdown vectors were transfected into 293T/17 cells with PEI. Virus-containing supernatant was passed through a 0.45μm filter and ultracentrifuged at 15,000 g for 2 hr. Organoids were first dissociated into single cells prior to infection with the lentivirus and then selected with puromycin, as previously described (Huch et al., 2015).

CRISPR/Cas9 knockout

The gRNA-coding cDNAs for human PRMT6 gene were designed and synthesized to make the lenti PRMT6-gRNA-Cas9 constructs. Briefly, the 24bp forward and reverse primers including 20bp target sequence and BsmbI sticky end were annealed and inserted into the lentiCRISPR-v2 plasmid (Addgene 52961) digested with BsmbI (Fermentas). Primer sequences are as follows: KO#1, forward, 5′-CACCGTGCTGCTGCGCTACAAAGT-3′and reverse, 5′-AAACACTTTGTAGCGCAGCAGCAC-3′; KO#2, forward, 5′-CACCGCCCATCCACTCGCTCACGA-3′ and reverse, 5′-AAACTCGTGAGCGAGTGGATGGGC-3′. Sequences (0.5 μg) were transfected into 293T cells and packaged using 1 μg pMDL + 1 μg pRSV + 1 μg pVSVG (Addgene). Virus-containing supernatants were collected for subsequent transduction to establish cells with PRMT6 knocked out. Puromycin was used for cell selection.

Immunohistochemistry

Slides were heated for antigen retrieval in 10mM sodium citrate (pH 6.0). Endogenous peroxidase activity was inhibited with 3% hydrogen peroxide. Sections were subsequently incubated with anti-human/mouse PRMT6 (1:1000 for human, 1:100 for mouse, Abcam, ab47244), anti-human PRMT6 (1:300, Atlas Antibodies, HPA059424), anti-mouse SOX2 (1:100, R&D Systems, MAB2018) and anti-mouse p-ERK1/2 (1:100, Abcam, ab50011). Reaction was developed with DAB+ Substrate-Chromogen System (Dako). Slides were counterstained with Mayer's hematoxylin.

Immunofluorescence

Cells were fixed with 4% paraformaldehyde, permeabilized with 0.1% Triton X (Sigma-Aldrich), blocked with normal goat serum and incubated with anti-human PRMT6 (1:1000, Abcam, ab47244) or anti-human PRMT6 (1:1000, Atlas Antibodies, HPA059424), followed by Alexa Fluor conjugated secondary antibody. Cells were counterstained with anti-fade DAPI (Invitrogen) and visualized by fluorescent confocal microscope (Carl Zeiss LSM 700).

Oncosphere-forming and self-renewal assay

Single cells were cultured in 300μl of serum-free DMEM/F12 medium (Invitrogen) supplemented with 20ng/ml human recombinant epidermal growth factor (Sigma-Aldrich), 10ng/ml human recombinant basic fibroblast growth factor (Sigma-Aldrich), 4μg/ml insulin (Sigma-Aldrich), B27 (1:50; Invitrogen), 500U/ml penicillin, 500μg/ml streptomycin (Invitrogen) and 1% methylcellulose (Sigma-Aldrich). Cells were cultured in suspension in poly-HEMA-coated 24-well plates. Cells were replenished with 30μl of supplemented medium every second day. To propagate spheres *in vitro*, spheres were collected by gentle centrifugation and dissociated to single cells using TrypLE Express (Invitrogen). Following dissociation, trypsin inhibitor (Invitrogen) was used to neutralize the reaction, and the cells were cultured to generate the next generation of spheres.

Cell motility and invasion assays

Migration and invasion assays were conducted in 24-well Millicell hanging inserts (Millipore) and 24-well BioCoat Matrigel Invasion Chambers (BD Biosciences), respectively. Cells re-suspended in serum free DMEM were added to the top chamber and medium supplemented with 10% FBS was added to the bottom chamber as a chemoattractant. After 48 hr of incubation at 37°C, cells that migrated or invaded through the membrane (migration) or Matrigel (invasion) were fixed and stained with crystal violet (Sigma-Aldrich). The number of cells was counted in 3 random fields under 20x objective lens and imaged using SPOT imaging software (Nikon).

Annexin V apoptosis assay

Cells were treated with various concentrations of chemo and molecular targeted therapeutic drugs, 5-fluorouracil, cisplatin and sorafenib for 2 days. Following treatment, cells were harvested and stained with propidium iodide (PI) and FITC-conjugated Annexin V as provided by the Annexin V-FLUOS Staining Kit (Roche). Samples were analyzed on BD FACSCanto II (BD Biosciences) with data analyzed by FlowJo (Tree Star Inc.).

Cell viability assay

Organoids were treated with various concentrations of chemo and molecular targeted therapeutic drugs, 5-fluorouracil, cisplatin and sorafenib for 4 days. Cell viability was measured by CellTiter-Glo assay (Promega) with data presented as percentage of viability relative to blank or vehicle control.

Tandem affinity purification – mass spectrometry

Affinity purification of PRMT6 protein complexes was carried out as described previously (Feng et al., 2016) on whole cell lysates. Stable clones of 293T cells expressing PRMT6 with C-terminally tagged with SFB were harvested and lysed in NETN buffer for 30 mins on ice. After removal of cell debris by centrifugation at 14k rpm for 15 mins, supernatant containing PRMT6-protein complexes was first immunoprecipitated by streptavidin bead slurry (Amersham) for 4 hr at 4°C. The precipitated protein complexes were then eluted by incubation with NETN buffer containing 2mg/ml biotin (Sigma-Aldrich). The biotin-eluate was then incubated with S protein agarose (Novagen) for 3 hr to perform a second round of immunoprecipitation. The protein complexes were eluted by heating at 95°C for 5 mins. The eluate was subjected to mass spectrometric analysis (LC/MS/MS) at Taplin Mass Spectrometry Facility (Harvard).

Methylation assays

For *in vivo* methylation, 293T cells were co-transfected with HA-FLAG-CRAF and PRMT6 plasmids. 48 hr later, the cells were lysed by NETN buffer and immunoprecipitation was performed to pull down the HA-FLAG-tagged CRAF protein. The input and eluted protein lysates were resolved by SDS-PAGE and analyzed by western blotting. The level of asymmetric dimethylated arginine in HA-FLAG-CRAF was assessed by using anti-ADMA (1:1000, Cell Signaling, 13522). For *in vitro* methylation assay, SFB-PRMT6 protein was immunoprecipitated from crude extract of 293T stable clones. 293T-CMV-SFB stable cells were used as control. The substrate GST-CRAF was purified from transformed BL21 competent *E. coli*. Quantity of input lysates for IP was normalized by measurement of protein concentration and also by SDS-PAGE and subsequent Coomassie blue staining. Equal amount of immobilized SFB-PRMT6 or CVM-SFB was mixed with 1 μg of GST-CRAF in the presence of 1 μCi of [methyl-^{3}H] S-adenosyl-L-methionine (Amersham) and 25mM Tris-HCl (pH 7.5) for 2 hr at 30°C in a final volume of 50μl. Reactions were stopped by adding 20μl of 2x Laemmli buffer, followed by heating at 100°C for 5 mins. Products were loaded into SDS-PAGE and analyzed by western blotting. The radioactive signals from GST-CRAF were visualized by fluorography with En^{3}Hance (Perkin-Elmer) according to manufacturer's instructions. For *in vitro* peptide methylation, SFB-PRMT6 protein was immunoprecipitated from crude extract of 293T stable clones. Enzyme was then incubated with either 100 μg of unmodified CRAF R100 peptide (CAVFRLLHE), or modified CRAF R100K (CAVFKLLHE) (GenScript Inc.) in the presence of 1 μCi of [methyl-^{3}H] S-adenosyl-l-methionine (Amersham) for 2 hr at 30°C in a final volume of 50 μL of methylation buffer [100 mM Tris-HCl (pH 8.0), 1mM EDTA, and 1mM DTT]. Peptides were loaded onto filter papers, washed and counted by liquid scintillation.

Liquid chromatography–mass spectrometry analysis

SFB-PRMT6 was incubated with 100 μg of CRAF R100 peptide in the presence of 500ng *S*-(5′-Adenosyl)-L-methionine chloride dihydrochloride (Sigma-Aldrich) for 2 hr at 30°C in a final volume of 50 μL methlylation buffer. Peptides were purified with ZipTip C18 pipette tips (Millipore). 8 μg was analyzed by liquid chromatography-mass spectrometry and mass spectrometry (LC-MS/MS) on Orbitrap Fusion Lumos Tribid Mass Spectrometer (Thermo Scientific) at the Proteomics & Metabolomics Core Facility, The University of Hong Kong. Data analysis was performed using PEAKS DB software (Bioinformatics Solutions Ltd).

In vitro RAS binding assay

For RAS preparation, MBP-RAS was purified from transformed BL21 competent *E. coli.* and loaded with 0.1M GTP$_\gamma$S for 30 mins at 30°C. Reaction was stopped by addition of $MgCl_2$ to a final concentration of 20mM. For *in vitro* methylation and sequential RAS binding assay, equal amount of GST-CRAF or GST-CRAF-R100K was incubated with immobilized SFB-PRMT6 and 1 μCi of [methyl-^{3}H] S-adenosyl-L-methionine (Amersham) at for 2 hr at 30°C in a final volume of 50 μL methylation buffer. The reaction supernatant was then incubated with MBP-RAS-GTP$_\gamma$S and Glutathione Sepharose for 2 hr at 4°C. After washing the beads, the reaction products were analyzed by western blotting.

ChIP-qPCR

ChIP was performed with the Magna ChIP G – Chromatin Immunoprecipitation Kit (Millipore) according to manufacturer's instructions. Briefly, cells were crosslinked in the presence of 1% formaldehyde at room temperature for 10 min and harvested after washing with cold PBS. Immunoprecipitation of crosslinked protein/DNA was carried out with 4 μg of anti-histone H3 (asymmetric di

methyl R2) antibody (Abcam, ab175007) or rabbit IgG control (Santa Cruz, sc-2027). Immunoprecipitated and eluted DNA was purified with columns and amplified by qPCR with the following primers: p21 promoter region, forward, 5′-TGCGTTCA CAGGTGTTTCTG-3′ and reverse, 5′-CACATCCCGACTCTCGTCAC-3′; p27 promoter region, forward, 5′-ACTCGCCGTGTCAAT CATTT-3′ and reverse, 5′-AACACCCCGAAAAGACGAG-3′; p57 promoter region, forward, 5′-TCCAGCTCTCCAGCTTTTG-3′ and reverse, 5′- TCCAGTCTGTTTGTGCTTGTG-3′.

QUANTIFICATION AND STATISTICAL ANALYSIS

Statistical analyses were performed using GraphPad Prism 5.0 and SPSS 21.0. Independent Student's t test was used to compare the mean value of two groups. Clinico-pathological significance in clinical samples was evaluated by Fisher's exact test and independent Student's t test for categorical data and continuous data, respectively. The differences in survival were calculated using the Kaplan-Meier test. Survival analysis in mouse model was performed by log-rank test. Data representative of two or more independent experiments. Bars and error represent mean ± standard deviations (SD) of replicate measurements. Statistical significance was defined as $p \leq 0.05$. *$p < 0.05$, **$p < 0.01$ and ***$p < 0.001$. Number of animals included per group can be found in each respective Figure.

DATA AND SOFTWARE AVAILABILITY

Microarray gene expression data are deposited at the NCBI GEO under the accession number GEO: GSE97931.